Supramolecular Chemistry

ISSN: (Print) (Online) Journal homepage: https://www.tandfonline.com/loi/gsch20

Self assembled cages with mechanically interlocked cucurbiturils

Kimberly G. Brady, Bingqing Liu, Xiaopeng Li & Lyle Isaacs

To cite this article: Kimberly G. Brady, Bingqing Liu, Xiaopeng Li & Lyle Isaacs (2021) Self assembled cages with mechanically interlocked cucurbiturils, Supramolecular Chemistry, 33:1-2, 8-32, DOI: 10.1080/10610278.2021.1908546

To link to this article: https://doi.org/10.1080/10610278.2021.1908546

SUPRAMOLECULAR CHEMISTRY
2021, VOL. 33, NOS. 1–2, 8–32
https://doi.org/10.1080/10610278.2021.1908546

Taylor & Francis
Taylor & Francis Group

Self assembled cages with mechanically interlocked cucurbiturils

Kimberly G. Brady[a], Bingqing Liu[b], Xiaopeng Li[b] and Lyle Isaacs[a]

[a]Department of Chemistry and Biochemistry, University of Maryland, College Park, Maryland, USA; [b]Department of Chemistry, University of South Florida, Tampa, Florida, USA

ABSTRACT

We report (bis)aniline **4** which contains a central viologen and its self-assembly with aldehyde **5** and $Fe(OTf)_2$ to yield tetrahedron **6**. Complexation of **4** with CB[7] in the form of CB[7]•**4**•$2PF_6$ allows the preparation of assembly **7** which contains 1.95 mechanically interlocked CB[7] units. Assemblies **6** and **7** are hydrolytically unstable due to their imine linkages. Redesign of our system with water stable 2,2′-bipyridine end groups was realised in the form of ligands **11** and **16**. Self-assembly of **11** with $Fe(NTf_2)_2$ gave tetrahedral MOP **12**. Isomeric ligand **16** underwent self-assembly with $Fe(OTf)_2$ to give cube **17**. Precomplexation of ligands **11** and **16** with CB[7] gave the acetonitrile soluble CB[7]•**11**•$2PF_6$ and CB[7]•**16**•$2PF_6$ complexes. Self-assembly of CB[7]•**11**•$2PF_6$ with $Fe(OTf)_2$ gave tetrahedron **13** which contains 1.8 mechanically interlocked CB [7] units. Self-assembly of CB[7]•**16**•$2PF_6$ with $Fe(OTf)_2$ gave cube **13** which contains 6.59 interlocked CB[7] units.

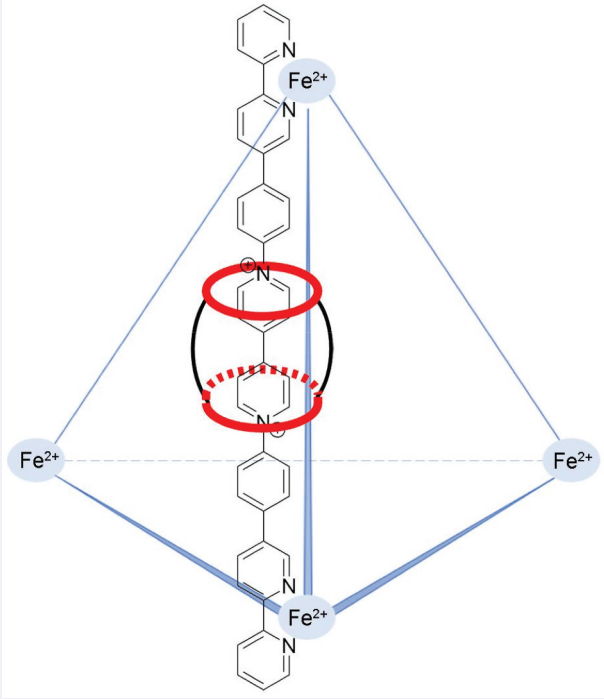

ARTICLE HISTORY
Received 28 January 2021
Accepted 22 March 2021

KEYWORDS
Cucurbit[n]uril; metal organic polyhedra; self-assembly; mechanical interlocked compounds

Introduction

A wide variety of molecular container compounds have been studied over the past decades including cyclodextrins, cyclophanes, calixarenes, cavitands, and more recently cucurbit[n]uril (CB[n]) and pillararenes (Figure 1) [1–9]. When molecular containers bind guest compounds within their cavity, they can fundamentally alter their optical properties (e.g. UV/Vis, fluorescence), physical properties (e.g. solubility, vapour pressure), chemical properties (e.g. conformation, reactivity, pK_a), and even their biological properties [10–17]. Accordingly,

CONTACT Lyle Isaacs LIsaacs@umd.edu Department of Chemistry and Biochemistry, University of Maryland, College Park, Maryland 20742, USA
Supplemental data for this article can be accessed here.

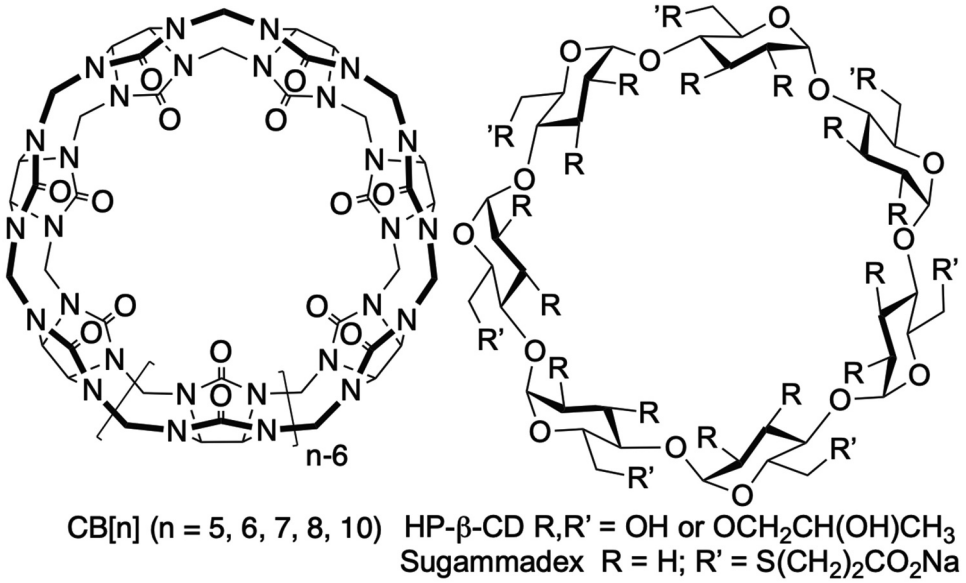

Figure 1. Structures of cyclodextrins and cucurbit[n]urils.

molecular containers have been used in numerous applications including as supramolecular catalysts, as components of separations processes, as components of sensing ensembles, as components of smart materials and molecular machines, and to construct drug delivery systems [18–25]. Amongst these molecular containers, cyclodextrin derivatives have found a wide variety of practical real world applications including the formulation of insoluble pharmaceuticals for human use, as the active ingredient in the household product Febreeze™, and as an *in vivo* reversal agent for rocuronium and vecuronium in the form of Sugammadex [26–29].

Our group has been most interested in the chemistry of the CB[n] family of molecular container compounds (Figure 1) [1,30–33]. CB[n] are composed of *n* glycoluril repeat units connected by 2 *n* methylene bridges which define a central hydrophobic cavity and two symmetry equivalent ureidyl carbonyl portals that are regions of highly negative electrostatic potential [34]. Accordingly, CB[n] hosts bind to a wide variety of guest molecules that present hydrophobic and cationic functionality including the N-terminus of peptides and proteins, cationic dyes, alkyl and aryl (di)ammonium ions, neurotransmitters, active pharmaceutical ingredients, drugs of abuse, and electrochemically active guests like ferrocene and viologen derivatives [35–44]. Advantageously, CB[n]-type receptors typically display high *in vitro* and *in vivo* biocompatibility [45]. Compared to other molecular containers, CB[n]-type hosts are special because they display high affinity and highly selective binding events in water (K_a commonly 10^6 M^{-1}; K_a up to 10^{17} M^{-1}) [33,46]. Because CB[n]•guest complexes are so selective they are responsive towards chemical, pH, photochemical, and electrochemical stimuli [43,44,47,48]. For all these reasons, CB[n]-type containers have been used in a variety of applications including chemical sensing, promotors of protein dimerisation, drug formulation, delivery and sequestration, separations materials, and to construct molecular machines and devices [33,37,49–52]. CB[n] are even beginning to appear in household deodorising products [53].

Self-assembly processes driven by hydrogen bonding [54], the hydrophobic effect [55], or metal-ligand interactions [56–60] represent powerful alternative approaches towards functional molecular container compounds. Metal-ligand coordination-driven self-assembly has been particularly widely employed due to the well defined geometry of the metal coordination sphere and the strength of the metal-ligand interactions which lead to more predictable self-assembly processes. The vibrant fields of metal organic frameworks (MOF) and metal organic cages fall within the category of molecular containers self-assembled via metal-ligand interactions. MOFs are extended solids that have been used for a variety of applications including as materials for hydrogen storage, water and gas capture and separation, carbon capture and sequestration, biological imaging and sensing, and drug delivery processes [59,61,62]. The Loeb and Stoddart groups have studied the incorporation of macrocycles into MOFs and studied their dynamic and host-guest recognition properties [63–66]. Related supramolecular organic frameworks (SOFs) incorporating CB[n] have been developed in recent years by the Li group [67–69]. Very recently, Trabolsi has reported a covalent organic framework containing mechanically interlocked CB[7] units [70]. Conversely,

metal organic cages are discrete self-assembled structures that are soluble in organic or aqueous solution whose properties can be tailored by altering the structures of the constituent building blocks. Metal organic cages have been used for basic studies of molecular recognition processes, to tame highly reactive species (e.g. P_4), as catalysts, for sensing and imaging, for drug delivery, and even as therapeutics themselves [56,58,71–74].

Several years ago, we saw the opportunity to integrate the desirable molecular recognition properties and stimuli responsiveness of CB[n] hosts with the desirable structural features of metal organic polyhedra (MOP) to create multivalent architectures that would be particularly well suited towards (targeted) therapeutic and imaging applications. Towards this goal, we reported the synthesis of bis(pyridyl) ligand **L1** and its self-assembly with $Pd(NO_3)_2$ to yield the cubooctahedral Fujita type sphere **A1** which is studded with 24 methyl viologen (MV) units (Scheme 1) [75]. The methyl viologen units of **A1** allow the primary recruitment of CB[8] to form CB[8]•MV binary complexes which can undergo subsequent ternary complex formation with a naphthol functionalised doxorubicin prodrug. The results of MTS assays showed that **A1** exhibited 10-fold higher cytotoxicity towards HeLa cancer cells than an equivalent amount of doxorubicin prodrug alone which

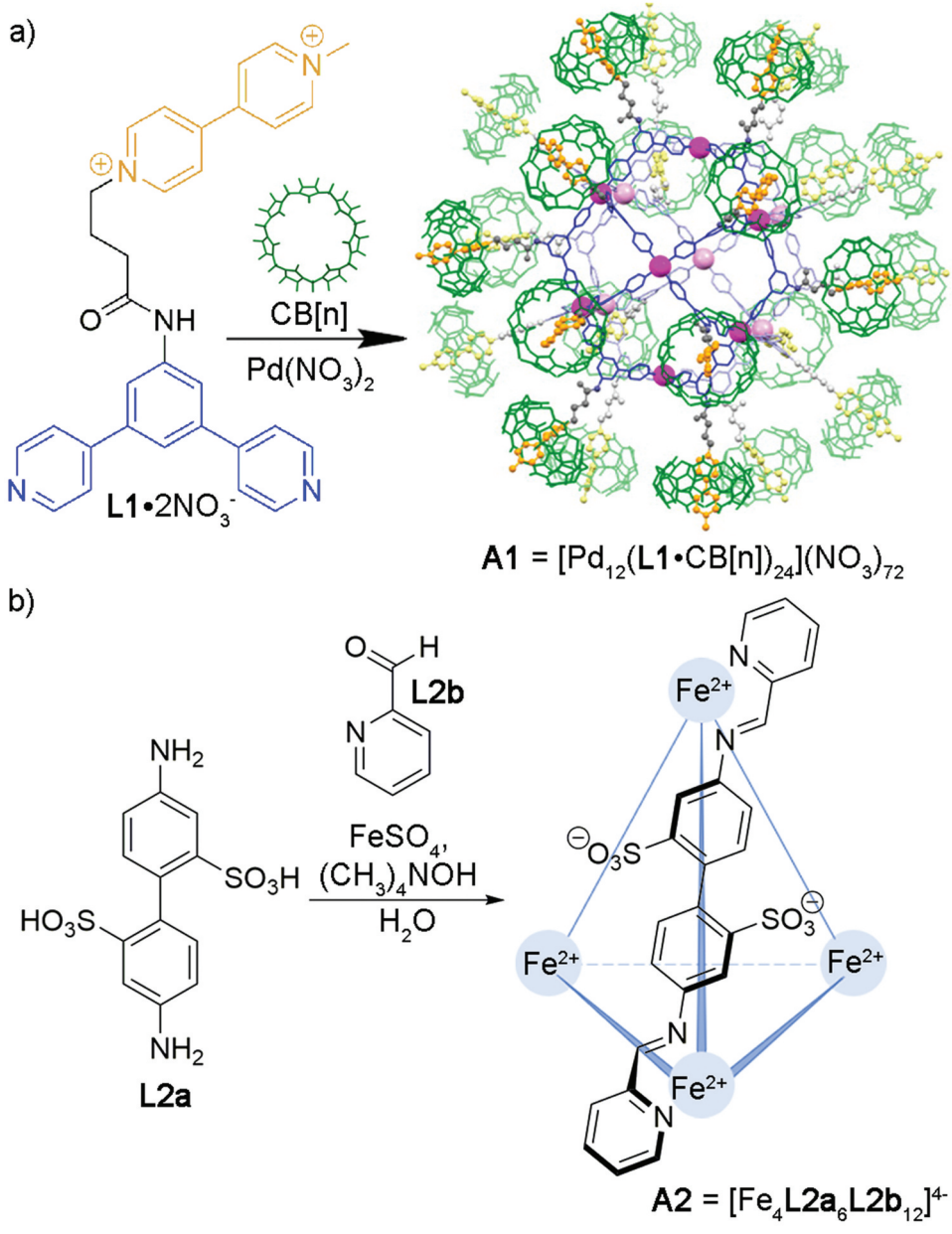

Scheme 1. (a) Self-assembly of palladium MOP conjugated with CB[n]s. (b) Self-assembly of water-soluble iron-based tetrahedra utilising dynamic covalent coordinative bonds developed by the Nitschke group.

could be traced to the enhanced cellular uptake of the larger (≈ 6 nm) multivalent MOP-CB architecture. In follow up work we showed that related Fujita-type MOPs could be covalently functionalised with CB[7] and co-functionalised *via* click chemistry with dyes (e.g. fluorescein, cyanine 5.5), targeting ligands (e.g. biotin, RGD), and PEG groups [76,77].

Despite these advances, the Fujita type systems are made using transition metals such as palladium and platinum which can be cytotoxic on their own. Furthermore, the non-covalent attachment of the CB[n] units discussed above was deemed less attractive for future *in vivo* biomedical application due to the potential for premature decomplexation. Accordingly, we envisioned that related MOP architectures based on biocompatible metals that feature either mechanically interlocked or covalently connected CB[n] would be desirable. We were drawn to the pioneering work of Nitschke and co-workers who have developed iron-based metal organic cages that are based on subcomponent self-assembly of iron salt, aniline derivatives, and aryl aldehydes (e.g. $FeSO_4$ + **L2a** + **L2b**; Scheme 1) [78,79]. Nitschke has created water soluble versions of these metal organic cages, demonstrated their biocompatibility, and their use in materials science (e.g. hydrogels) and for uptake and release applications [80–84]. Accordingly, we decided to explore a strategic merger of the structural features of iron based MOPs with the recognition properties of CB[n]. In this paper we report our work directed towards the preparation of iron based Nitschke type MOPs with mechanically interlocked CB[n] units which was envisioned to allow uptake and release of drugs within a multivalent architecture.

Results and discussion

This results and discussion section is organised as follows. First, we describe the self-assembly of Nitschke-type tetrahedron **6** by the self-assembly of viologen dianiline **4** and aldehyde **5** in the presence of $Fe(OTf)_2$ and the threading of CB[7] to yield tetrahedron **7** with mechanically interlocked CB[7] units. Next, we describe the preparation of analogous viologen bipyridine ligands **11** and **16** and their self-assembly with Fe^{II} salts in CH_3CN to deliver tetrahedra **12** and **13** and cubes **17** and **18**.

Synthesis of dianiline ligand 4 with viologen binding binding domain

In order to create a self-assembled MOP that features CB[n] binding domains according to Nitschke's subcomponent self-assembly strategy required the preparation of a linear dianiline containing a CB[n] binding domain. For this purpose, we designed compound **4** (Scheme 2) which features a central viologen unit which was introduced to the CB[n] field by Kaifer and Kim as an excellent guest for the CB[7] and CB[8] hosts [34,43,44,85–88]. Compound **1** was prepared by reaction of 4,4-bipyridine with 2,4-dinitrofluorobenzene in anhydrous CH_3CN according to a literature procedure [89]. Separately, benzidine was reacted with $(Boc)_2O$ to deliver **2** as described in the literature [90]. Subsequently, **1** was heated with 2.0 equiv. **2** in refluxing EtOH overnight followed by addition of THF which caused **3** to precipitate in 96% yield; this type of reaction is referred to as the Zincke reaction [91]. Finally, the t-butoxycarbonyl groups of **3** were deprotected by treatment with CH_3CO_2H (TFA) in CH_2Cl_2 to deliver **4** as its chloride salt in 98% yield. In accord with its high symmetry, Figure 2(a) shows the ^1H NMR spectrum recorded for **4** in CD_3CN which shows two ^1H NMR resonances for the symmetry equivalent viologen protons at 9.22 and 8.64 ppm (H_e and H_f, respectively) and four additional resonances (H_a – H_d) for the phenylene spacer and terminal aniline rings. The ^{13}C NMR spectrum of **4** shows 11 resonances in the aromatic region as expected based on symmetry considerations.

Self-assembly of nitschke-type tetrahedron 6

With dianiline ligand **4**•2Cl in hand, we sought to react it with pyridine-2-carboxyaldehyde (**5**) and $FeSO_4$ in water to deliver self-assembled tetrahedron **6**. Unfortunately, under aqueous conditions no product was formed which in retrospect is due to the hydrolysis of the labile imine linkages [92]. Accordingly, we performed counterion exchange of **4** from the chloride salt to the PF_6 salt by treatment of an aqueous solution of **4** with NH_4PF_6 to precipitate **4**•2PF_6 (Scheme 2). Compound **4**•2PF_6 is soluble in CH_3CN. Next, we performed the self-assembly reaction of a solution of **4**•2PF_6, **5**, and $Fe(OTf)_2$ in dry acetonitrile at 60°C for 24 hours (Scheme 3). Upon addition of $Fe(OTf)_2$, an immediate colour change from dark brown to deep purple was observed. UV/Vis spectroscopy shows the presence of a new absorption band from 500–615 nm (Supporting Information, Figure S31). This dramatic colour change is commonly observed during the formation of Nitschke-type cages due to the metal-to-ligand charge-transfer interactions associated with low-spin Fe^{II} in a hexaimine ligand environment [93]. The ^1H NMR spectra of tetrahedron **6** is shown in Figure 2(b) which displays a total of 10 aromatic CH

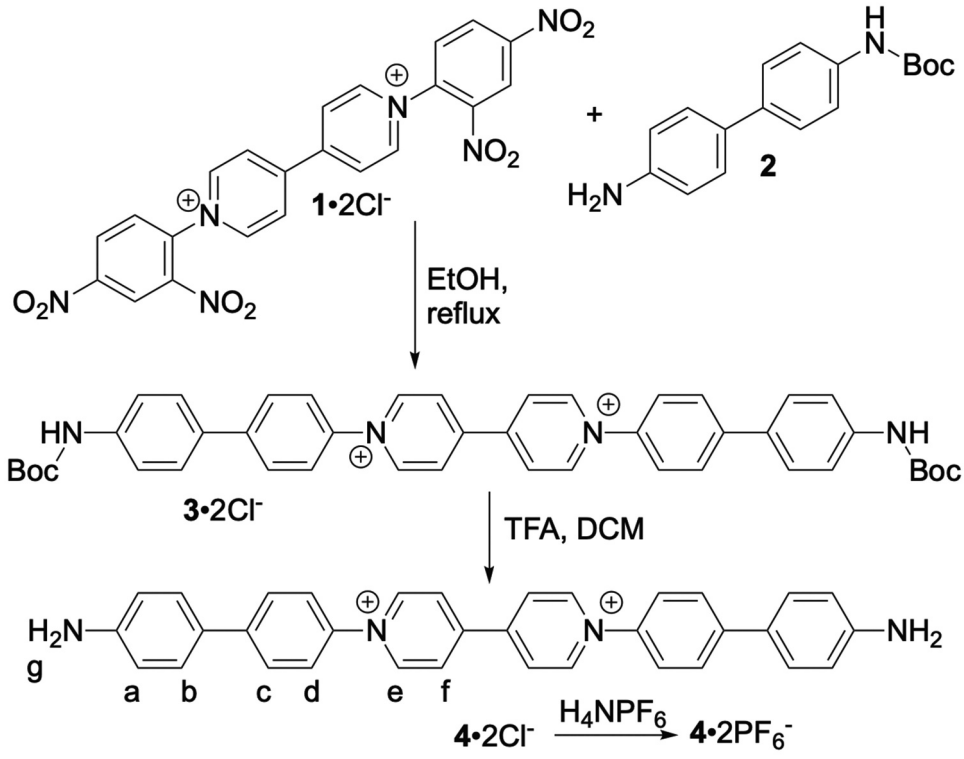

Scheme 2. Synthesis of dianiline ligand **4** as its chloride and PF_6 salts.

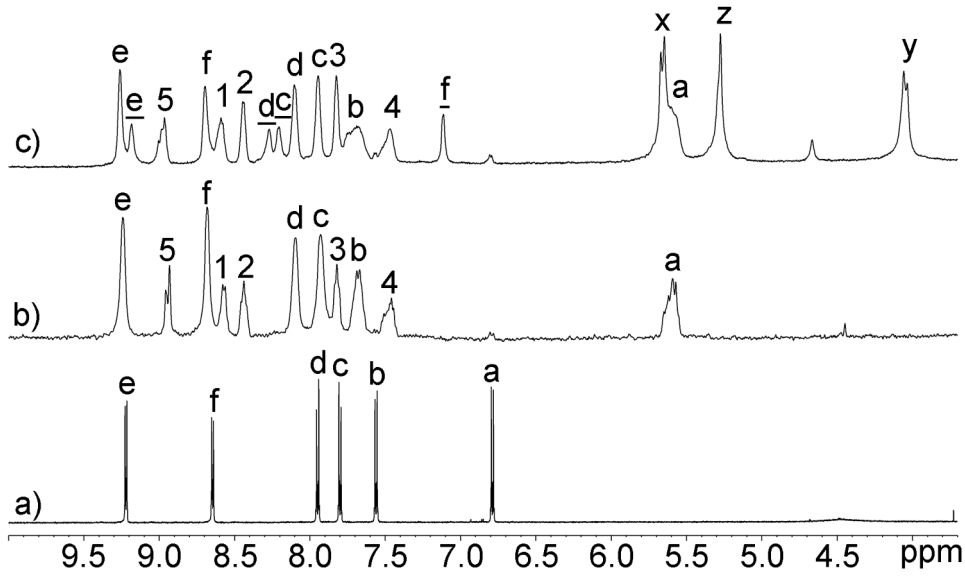

Figure 2. ^{1}H NMR spectra recorded (600 MHz, CD_3CN, RT) for: (a) **4**•2PF_6, (b) **6**•20PF_6, and (c) **7**•20PF_6. The resonances marked with an underscore (_) denote protons on ligand that contain mechanically interlocked CB[7] .

resonances and one imine CH resonance in accord with the depicted structure. The assignments of H_1 – H_4 to the pyridine portion of cage **6** and H_a – H_f to the extended viologen region of cage **6** was determined by the cross peaks in the two dimensional COSY spectrum (Supporting Information, Figure S22). The resonance for H_a undergoes a dramatic upfield shift (Figure 2(a,b)) from 6.79 ppm to 5.60 ppm which is diagnostic of self-assembly because H_a is in the anisotropic shielding region of an adjacent ligand at the Fe corner. Importantly, the resonance at 8.84 ppm is characteristic of the newly formed imine bond (HC = N) group. Nitschke has shown that this resonance is particularly sensitive to the presence of

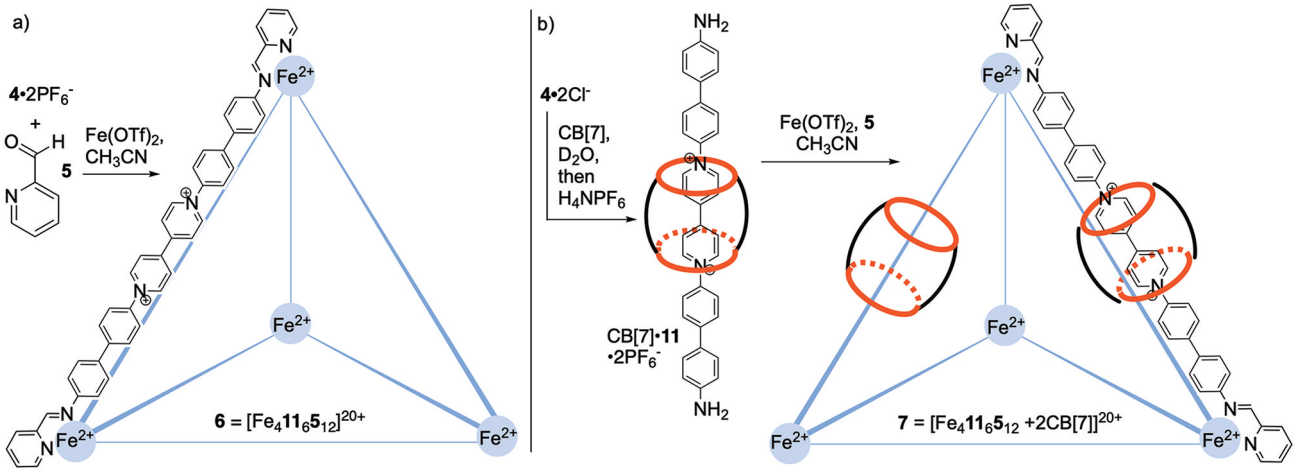

Scheme 3. Self-assembly of Nitschke-type tetrahedron **6** and its analogue **7** with mechanically interlocked CB[7].

diastereomers of the self-assembled tetrahedral cage [94,95]. Each metal ion corner of **6** can possess either the Δ or Λ stereochemistry which leads to 3 possible combinations (ΔΔΔΔ, ΔΔΔΛ, and ΔΔΛΛ) and their enantiomers. Figure 2(b) shows the presence of two peaks for H_5 at 8.97 and 8.94 ppm which indicates the presence of at least two diastereomeric forms of **6** are formed. Unfortunately, we were unable to obtain either an x-ray crystal structure or observe a parent ion by electrospray ionisation mass spectrometry for **6**. Accordingly, we turned to diffusion ordered spectroscopy (DOSY) to obtain information about the size of **6** [96]. The diffusion coefficient of **6** was measured as D = 3.68 x 10^{-10} m^2 s^{-1} in CD_3CN at 298 K which is 4.7-fold lower than that measured for dianiline **4** (D = 1.74 x 10^{-9} m^2 s^{-1}) under identical conditions which indicates formation of a significantly larger species. We used the Stokes-Einstein equation [96,97] to calculate the hydrodynamic diameter for **6**•20PF_6 as 34.6 Å. We created an MMFF94s minimised molecular model of **6** and measured the distance from the centroid of the four Fe centres to the furthest point of the assembly (22.1 Å) which gives a diameter of 44.2 Å which is slightly larger than that determined by DOSY. This discrepancy may be due to the fact that the assembly is tetrahedral rather than spherical. The diffusion coefficient measured for **6** is slightly smaller than that measured by Nitschke for an assembly constructed from an 2,6-bis(4-aminophenyl)anthracene

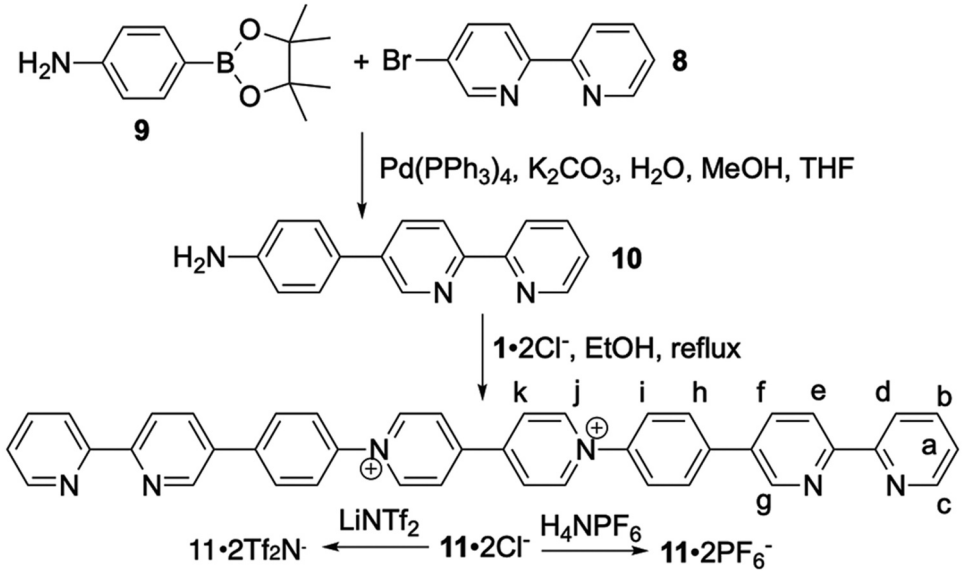

Scheme 4. Synthesis of modified bipyridyl ligand **11.**

based ligand (D = 3.82 x 10^{-10} m^2 s^{-1}) [95] which provides added support for our formulation of the tetrahedral geometry shown in Scheme 4.

Investigation of the complexation of dianiline 4 with CB[n] (n = 7, 8)

The ultimate goal of this project is to create a mechanically interlocked scaffold with CB[8] units on the edges of the MOP that will allow complexation of a multiplicity of drug molecules by the second binding site of CB[8] for drug delivery purposes. As a prelude to such studies, we performed separate titration experiments of dianiline ligand **4**•2Cl with CB[7] and CB[8] in D_2O. At a 1:1 stoichiometric ratio of **4**:CB[7], ^{1}H NMR spectroscopy (Supporting Information, Figure S11) shows that the resonances for H_e and H_f shift significantly upfield (H_e from 9.48 ppm to 9.20 ppm; H_f from 8.83 ppm to 7.86 ppm) compared to **4** alone. The cavity of CB[n] constitutes a magnetically shielding environment [98], which provides strong evidence that CB[7] resides on the central viologen in the CB[7]•**4** complex. As additional quantities of CB[7] is added, the ^{1}H NMR resonances for H_e and H_f shift back towards those observed for free **4** whereas the resonances for the terminal aniline units (H_a – H_d) shift upfield. At a 1:2 **4**:CB[7] stoichiometry a simple spectrum is observed which is indicative of a CB[7]•**4**•CB[7] complex where the CB[7] units reside on each terminal aniline unit. This change in binding site occurs when the free energy of CB[7] binding to two aniline units is larger than one CB[7] binding event at the central viologen unit. Subsequently, we attempted a titration experiment with CB[8] and **4**. Unfortunately, at equimolar ratios, we observed the immediate formation of a precipitate [99]. The small amount of material remaining in solution appears to be the $CB[8]_2$•$\mathbf{4}_2$ complex based on DOSY measurements (Supporting Information, Figure S17). It is well known that CB[8] can bind two aromatic guests simultaneously [44,85,100]. At a 1:1 CB[8]:**4** stoichiometric ratio, this opens up the possibility that CB[8] will bind two aniline termini in a head-to-tail fashion which ultimately leads to oligomerization. A 2:1 mixture of **4** and CB[8] was soluble in D_2O and the ^{1}H NMR showed that the aniline termini were encapsulated inside CB[8] (Supporting Information, Figure S15). Although we were disappointed by our inability to obtain a discrete 1:1 CB[8]•**4** complex we decided to move on towards the mechanical interlocking of CB[7] onto the edges of tetrahedron **6**.

Incorporation of mechanically interlocked CB[n] onto the edges of assembly 6 to create assembly 7

Given our successful formation of the CB[7]•**4** complex where the central viologen binding domain is complexed, we turned our efforts towards mechanically interlocking CB[7] on the edges of **6** (Scheme 3(b)). Initially, we tried to perform the one-pot self-assembly of a 6:12:4:6 mixture of **4**•2Cl, **5**, $FeSO_4$, and CB[7] in water but were unsuccessful. Based on the precedent of Nitschke [92], we also explored the addition of K_2SO_4 to increase ligand solubility and product stability and separately tested $Fe(OTf)_2$ as the iron source, but were uniformly unable to detect any self-assembled tetrahedral assembly. We surmise that the product is hydrolytically unstable under aqueous conditions, or that the iron salt may preferentially interact with the portals of CB[7] which disfavours the desired assembly pathway. Accordingly, we decided to perform the self-assembly process in CH_3CN as was successful for **6**. First, we created the discrete 1:1 CB[7]•**4** complex by mixing equimolar amounts of CB[7] and **4**•2Cl in water, followed by the addition of excess NH_4PF_6 or $LiNTf_2$ which causes the precipitation of the CB[7]•**4**•$2PF_6$ or CB[7]•**4**•$2NTf_2$ salts. The use of counterion exchange to solubilise CB[7] complexes in organic solution was first reported by Kaifer [88]. CB[7]•**4**•$2PF_6$ and CB[7]•**4**•$2NTf_2$ are soluble in CH_3CN and DMSO. Subsequently, self-assembly of a 6:12:4 mixture of CB[7]•**4**•$2PF_6$ salt, **5**, and $Fe(OTf)_2$ was performed in dry acetonitrile at 60 °C for 24 hours. The ^{1}H NMR spectrum recorded in CD_3CN (Figure 2(c)) shows two sets of peaks for each of the viologen protons (H_e, H_f) and each of the aniline protons (H_c, H_d) in a 1.95:1 ratio as determined by integration. Of particular note is that $\underline{H_f}$ is upfield shifted by 1.57 ppm to 7.11 ppm whereas $\underline{H_c}$ and $\underline{H_d}$ are slightly downfield shifted (≈ 0.2–0.3 ppm) within assembly **7**•$20PF_6$ relative to assembly **6**•$20PF_6$. These changes in chemical shift are comparable to that observed during the formation of the CB[7]•**4** complex which is strong evidence for the mechanical interlocking of an average of 1.95 CB[7] molecules onto the cage **6** to give the depicted structure of cage **7**. Conversely, the major resonances for H_f, H_c, and H_d in **7** for the uncomplexed edges appear at chemical shifts that are comparable to that observed for **6**. Approximately two edges of **7** are complexed with CB[7] and four edges remain uncomplexed. The DOSY spectrum of **7**•$20PF_6$ shows the presence of a single species with a diffusion coefficient (D = 2.71 x 10^{-10} m^2 s^{-1}) with a diameter of 46.8 Å calculated according to the Stokes-Einstein equation. The calculated diameter of **7** is 12.2 Å larger than that of **6**•$20PF_6$ which is approximately twice the radius of CB[7] (8.0 Å) [30,34]. Unfortunately,

we were unable to obtain ESI-MS data for assembly **7**. We observe the precipitation of CB[7] during the self assembly of cage **7** which establishes that CB[7] can decomplex from CB[7]•**4** complex during the reaction. Related experiments conducted with lower amounts of CB[7] (e.g. three free **4** and three CB[7]•**4**), still lead to assembly **7**. Attempts to prepare **7** by a slippage [101] process involving heating **6** and CB[7] in CD_3CN (60 °C) were unsuccessful due to the insolubility of CB[7]. Having successfully mechanically interlocked least 2 CB [7] molecules onto the edges to create **7** we tested the stability of **7** in water as a precursor step to the envisioned use of these assemblies in drug delivery. When water was added to either assembly **6** or **7**, we observed the disappearance of the characteristic purple colour and the ^{1}H NMR displayed resonances for the starting materials **4** and **5**. In particular, the loss of the imine H_5 peak and the emergence of the aldehyde O = C-H resonance provide strong evidence that the cage underwent hydrolysis in water due to hydrolytic instability. Given this finding it appeared that the envisioned mechanical interlocking of CB[n] onto the edges of Nitschke-type assemblies was a dead end which prompted us to explore ligands whose assemblies would be stable in water.

Synthesis of bipyridine based viologen ligand 11 and its self assembly to give MOP 12

To circumvent the problems with the aqueous hydrolysis of the imine bonds that hold assembly **7** together, we redesigned our system using a more robust ligand that is not prepared in a subcomponent self-assembly process. We settled on ligand **11** which features 2,2′-bipyridine termini as ligands and a central viologen unit as the CB[n] binding domain (Scheme 4). First, we performed the Suzuki reaction between commercially available starting materials **8** and **9** using $Pd(Ph_3)_4$ as catalyst to deliver **10** in 92% yield [102]. Next, we allowed aniline **10** to react with **1** by a double Zincke reaction in refluxing EtOH to deliver target ligand **11**•2Cl in 97% yield. Compound **11** was fully characterised spectroscopically (^{1}H, ^{13}C, ESI-MS). For example, the ^{1}H NMR spectrum of **11** recorded in D_2O (Supporting Information, Figure S32) show the characteristic viologen protons (H_j and H_k) resonances at 9.50 ppm and 8.83 ppm, a pair of coupled doublets for the phenylene linker (H_i and H_h) at 8.14 ppm and 8.00 ppm, and the expected seven additional aromatic resonances (H_a – H_g) for the 2,2′-bipyridyl end groups (two triplets (H_a and H_b), a singlet (H_g), and three pairs of doublets (H_d – H_f)). In the ^{13}C NMR spectrum, all 17 resonances expected for **11** on the basis of its depicted C_{2v}-symmetric structure were observed experimentally. Compound **11**•2Cl could be transformed into the corresponding PF_6 or NTf_2 salts by treatment of aqueous solutions of **11**•2Cl with an excess of NH_4PF_6 or $LiNTf_2$ which resulted in precipitation of **11**•2PF_6 and **11**•2NTf_2 which are used in some of the self-assembly reactions described below.

Before proceeding to the self-assembly of **11**•2Cl we decided to test its complexation with CB[7] and separately with CB[8] in the absence of iron salts. Simple ^{1}H NMR spectroscopic titration shows that **11**•2Cl binds to CB[7] in D_2O (Supporting Information, Figure S42). At a 1:0.9 ratio of **11**:CB[7], we observe upfield changes in chemical shift for viologen protons H_j and H_k as well as phenylene protons H_h and H_i whereas the resonances for H_c and H_g which are on the 2,2-bipyridine end groups do not experience significant changes in chemical shift. This indicates that the CB[7] units in the CB[7]•**11** complex are not at a fixed location but rather shuttle between the phenylene and viologen binding sites. At a 1:2 **11**:CB[7] ratio, the resonances for the phenylene linker H_h and H_i undergo further upfield changes in chemical shift as the CB[7] units become localised on the phenylene binding sites to accommodate the presence of two molecules of CB[7]. Somewhat differently, the ^{1}H NMR spectrum of a 1:1 mixture of **11** and CB[8] (Supporting Information, Figure S46 and S47) shows only small shifting for the viologen protons H_j and H_k (H_j from 9.50 to 9.40 ppm, H_k from 8.83 to 8.96 ppm) whereas the phenylene protons undergo more substantial upfield shifts (H_h from 8.00 to 7.36 ppm; H_i from 8.14 to 7.60 ppm) upon complexation.

Encouraged by the ability to observe 1:1 complexation between **11** and CB[7] or CB[8], we moved on to the self-assembly studies. Initially, we performed the self-assembly of **11**•2PF_6 and $Fe(OTf)_2$ (6:4 molar ratio) in CH_3CN at 60 °C for 24 hours which delivers self-assembled tetrahedron **12**•20PF_6 (Scheme 5). Immediately after mixing, we observed a colour change from yellow-brown to red which is characteristic of the formation of the iron-bipyridine complex. Figure 3(a,b) shows the ^{1}H NMR spectra recorded for **11**•2PF_6 and for the self-assembled MOP **12**•20NTf_2. Upon self-assembly, the resonances for H_c and H_g which are adjacent to the bipyridine N-atoms undergo significant upfield shifts (H_c: 8.71 ppm to 7.50 ppm; H_g: 9.10 ppm to 7.79 ppm) which reflects that these protons feel the anisotropic shielding effect of an adjacent bipyridine when complexed to the metal centre [103,104]. Conversely, H_a, H_d, H_e, and H_f undergo slight downfield shifts upon self-assembly (H_a: 7.94 to 8.20 ppm, H_d: 8.29 to 8.50 ppm, H_e: 8.50 to 8.65 ppm, and H_f: 8.61 to 8.72 ppm) likely due to changes in the electronics of the bipyridine ring upon coordination to iron. In this case, the observation of a single set of sharp ^{1}H and ^{13}C NMR (Supporting Information, Figure

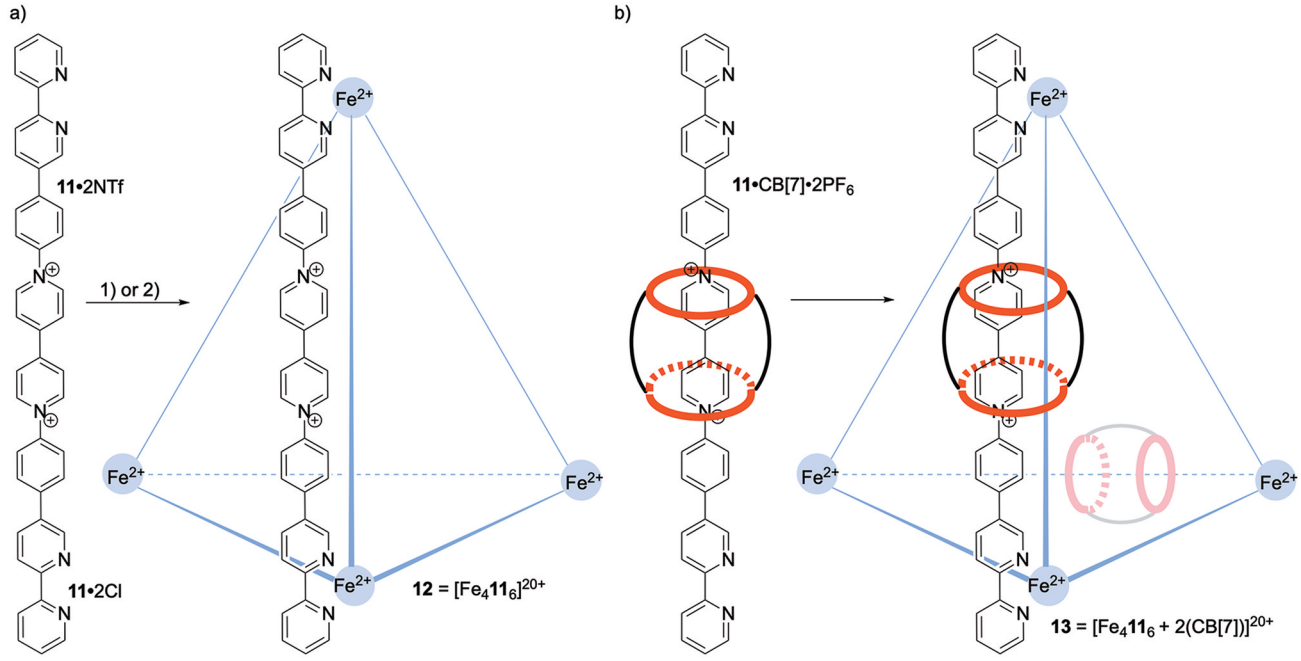

Scheme 5. Self-assembly of: (a) tetrahedron **12** performed in either CH_3CN or H_2O, and (b) tetrahedron **13** which incorporates CB[7] units. Conditions: 1) $Fe(NTf_2)_2$, CH_3CN, 60°C, 2) K_2SO_4, $FeSO_4$, 60°C.

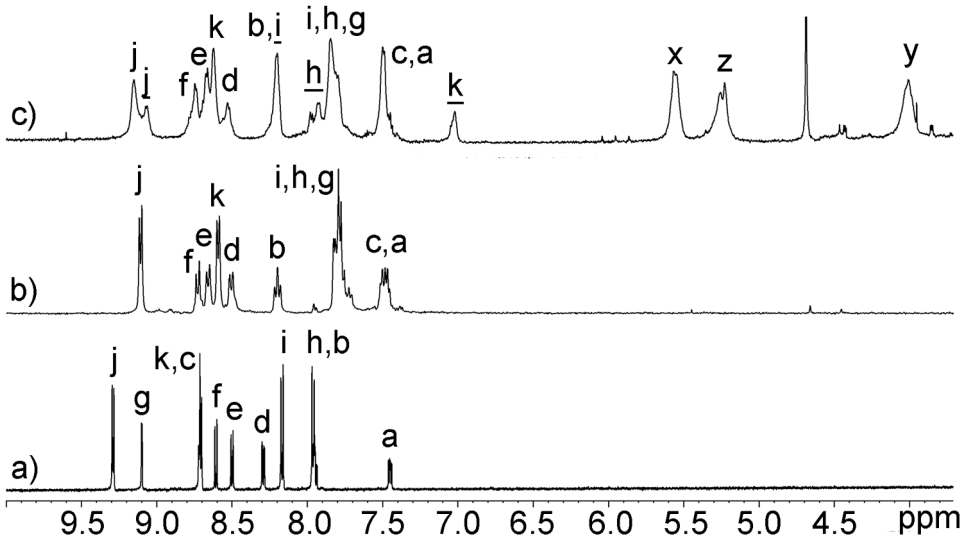

Figure 3. ^1H NMR spectra recorded (600 MHz, CD_3CN, RT) for: (a) **11**•$2PF_6$, (b) **12**•$20NTf_2$, and (c) **13**•$20PF_6$. The resonances marked with an underscore (_) denote protons on ligand that contain mechanically interlocked CB[7] .

S50) resonances of the expected number and multiplicity strongly suggests the formation of a single diastereomer of **12** which we formulate as the racemic mixture of ΔΔΔΔ-**12** and ΛΛΛΛ-**12**. The UV/Vis spectra recorded for **11** and assembly **12** in CH_3CN is given in the Supporting Information (Supporting Information, Figure S70). The spectra for **12** shows a new band with λ_{max} = 539 nm which is due to metal to ligand charge transfer upon complexation [104,105], as well as the shifting of a shorter wavelength λ_{max} from 294 (for **11**) to 315 nm (for **12**). We used DOSY NMR to determine the diffusion coefficient for **12**•$20PF_6$ in acetonitrile at 25 °C (D = 3.08 x 10^{-10} m^2 s^{-1}) as given in Table 1 which is 2.4-fold slower than the free ligand **11**•$2PF_6$ (D = 7.30 x 10^{-10} m/s^2) which provides support for self-assembly. The calculated hydrodynamic diameter of **12**•$20PF_6$ is 41.4 Å which is somewhat larger than Nitschke-type cage **6**•$20PF_6$ (34.6 Å) [106]. Finally, Figure 4(a) shows the electrospray ionisation mass spectrum recorded for assembly **12** as its PF_6 salt. We observe the presence of

Table 1. Diffusion coefficients (m/s^2) and calculated hydrodynamic diameters (Å) for the different ligands and self-assembled structures. Conditions: CD_3CN, 298 K.

Compound	$D_{MeCN}(m^2/s)$	Hydrodynamic Diameter (Å)
4•2PF_6	(1.74 ± 0.01) x 10^{-9}	7.3
4•CB7•2PF_6	(5.53 ± 0.28) x 10^{-10}	23.0
6•20PF_6	(3.68 ± 0.80) x 10^{-10}	34.6
7•20PF_6	(2.71 ± 0.07) x 10^{-10}	46.8
11•2PF_6	(7.30 ± 0.39) x 10^{-10}	17.4
11•CB7•2PF_6	(5.08 ± 0.38) x 10^{-10}	25.1
12•20PF_6	(3.08 ± 0.12) x 10^{-10}	41.4
13•20PF_6	(3.06 ± 0.15) x 10^{-10}	41.7
16•2PF_6	(7.71 ± 0.11) x 10^{-10}	16.5
16•CB7•2PF_6	(5.66 ± 0.34) x 10^{-10}	22.5
17•40PF_6	(1.40 ± 0.01) x 10^{-10}	91.3
18•40PF_6	(1.25 ± 0.24) x 10^{-10}	102

ions in the mass spectrum that correspond to the 6+ to 9 + ions of **12**•20PF_6 ($[Fe_4\mathbf{11}_6 + 14(PF_6)]^{6+}$ *m/z* = 994.23; $[Fe_4\mathbf{11}_6 + 13(PF_6)]^{7+}$ *m/z* = 831.35; $[Fe_4\mathbf{11}_6 + 12(PF_6)]^{8+}$ *m/z* = 709.30; $[Fe_4\mathbf{11}_6 + 11(PF_6)]^{9+}$ *m/z* = 614.38) upon successive loses of PF_6 counterions. The **12**•20PF_6 salt could be transformed to the **12**•10SO_4 salt by treatment of a CH_3CN solution with excess K_2SO_4 which gave the sulphate salt as a solid precipitate. MOP **12**•10SO_4 was soluble in water and did not undergo any change by ^{1}H NMR upon standing at 25 °C for > 2 weeks. MOP **12**•10SO_4 could also be synthesised directly under aqueous conditions from a 6:60:4 mixture of **11**•2Cl, K_2SO_4, and $FeSO_4$ by sonicating for 30 minutes at room temperature and then heating at 60°C for 24 hours (Scheme 5, Figure S57).

Mechanical interlocking of CB[n] onto the edges of cage 12 to give cage 13

Encouraged by the successful self-assembly of **12** under aqueous conditions, we decided to target the incorporation of mechanically interlocked CB[n] components. For this purpose, we performed the self-assembly of **11**•2Cl, CB[7], K_2SO_4, $FeSO_4$ (6:6:60:4) in water (60 °C) for 24 hours. The reaction mixture did not change colour over this time period as was expected and remained heterogenous throughout. Furthermore, we did not observe upfield shifting for H_c and H_g in the ^{1}H NMR spectrum which would be expected upon formation of the iron(bipyridine)$_3$ corners. Our interpretation is that the conformation heterogeneity of the **11**•CB[7] complex in water (e.g. mainly on the phenylene rather than the viologen binding site hinders formation of the targeted self-assembled cage perhaps by promoting protonation of the bipyridine units. In contrast, the ^{1}H NMR spectrum recorded in acetonitrile for the CB[7]•**11**•2PF_6 complex that had been prepared in water shows a substantial upfield shift for viologen resonance H_k from 8.71 ppm for free **11**•2PF_6 to 7.17 ppm as part of the CB[7]•**11**•2PF_6 complex which provides clear evidence for the CB[7] residing on the viologen unit (Supporting Information, Figure S43). Proton H_j also undergoes a small upfield shift upon complexation whereas the remaining protons on ligand **11** undergo small downfield changes in chemical shift. Accordingly, we next performed the self-assembly of a mixture of CB[7]•**11**•2PF_6 and $Fe(OTf)_2$ in acetonitrile at 60 °C for 24 hours (Scheme 5(b)). The self-assembly process is also successful when CB[7]•**11**•2NTf_2 and $Fe(NTf_2)_2$ are employed. The reaction mixture rapidly changes colour from yellow to ruby red. MOP **13**•20PF_6 was isolated after precipitation from the reaction mixture by the addition of Et_2O followed by centrifugation, decanting the supernatant, and drying. The ^{1}H NMR of **13**•20PF_6 recorded in CD_3CN is shown in Figure 3(c). The assignment of the resonances is based upon the correlations observed in the COSY spectrum (Supporting Information, Figure S65). Most strikingly, the resonance

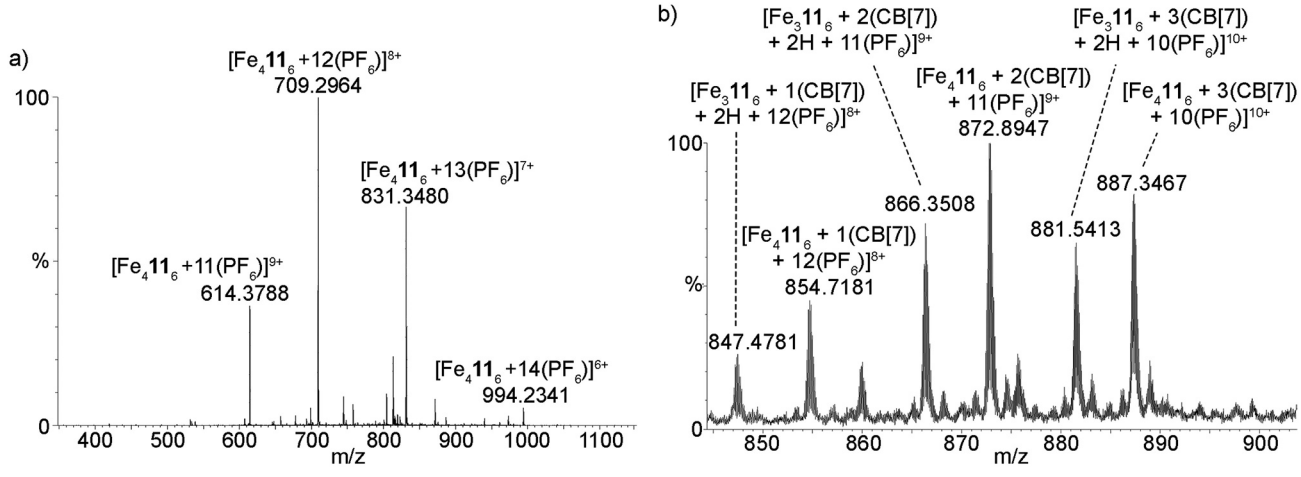

Figure 4. Mass spectra recorded for CH_3CN:DMSO solutions of: (a) **12**•20PF_6, and (b) **13**•20PF_6.

for viologen proton H_k in **13** shifts dramatically upfield to 7.02 ppm compared to that observed for **12** (8.59 ppm, Figure 2(b)) which lacks CB[7] units. Furthermore, we observe two sets of resonances for protons H_h, H_i, H_j, and H_k of unequal (1.80 by integration) ratio by ^{1}H NMR. This ^{1}H NMR data suggests that on average four **11** ligands that are part of assembly **13** do not have mechanically interlocked CB[7] units whereas two ligands of **11** possess a mechanically interlocked CB[7] unit. Integration of the resonances for the CB[7] unit (H_x, H_y, H_z) versus the ligand protons (H_j and $\underline{H_j}$ combined) also shows that 1.80 CB[7] are mechanically interlocked on **13**. The slight upfield shift observed for $\underline{H_j}$ (9.10 to 9.06 ppm) and the slight downfield shifts observed for $\underline{H_h}$ (7.80 to 7.97 ppm) and $\underline{H_i}$ (7.80 to 8.20 ppm) relative to H_j, H_h, and H_i support the notion that the CB[7] units reside on the viologen binding domain in assembly **13**. To gauge the size of assembly **13**•20PF_6 we performed DOSY NMR which allowed us to calculate the diffusion coefficient ($D = 3.06 \times 10^{-10}$ m/s^2) and the hydrodynamic diameter of assembly **13** (41.7 Å) in acetonitrile. The resonances for ligand **11** and CB[7] within assembly **13** diffuse at the same rate which provides further evidence for the interlocked nature of **13**. The diffusion coefficient and hydrodynamic radius of **13** are very similar to those measured for the Nitschke-type assembly **7** which also contains interlocked CB[7] units (Table 1). Figure 4(b) shows a region of ESI mass spectrum obtained for **13** as its PF_6 salt. We observe dominant ions at *m/z* 887.35 ([Fe_4 **11**$_6$ + 3(CB[7]) + 10(PF_6)]$^{10+}$), 872.89 ([Fe_4**11**$_6$ + 2(CB[7]) + 11(PF_6)]$^{9+}$), and 854.72 ([Fe_4**11**$_6$ + 1(CB[7]) + 12(PF_6)]$^{8+}$) which correspond to cage **13** with three, two, and one interlocked CB[7], respectively, as their 10+, 9+, and 8 + ions (Supporting Information, Figures S67 – S69). The combined inference of the ^{1}H NMR, DOSY, and ESI-MS data provides strong support for the formulation of **13** as a tetrahedral cage that possesses an average of 1.80, but a range of 1–3, mechanically interlocked CB[7] units. We also attempted the self-assembly of **11**•2Cl, $FeSO_4$, K_2SO_4, and CB[8] in water at 60 °C, but we did not observe any colour change which is strong evidence against the formation of iron(bipyridine)$_3$ complexes under these conditions. We suspect that the ureidyl C = O groups of CB[8] scavenge the $FeSO_4$ and prevent assembly. Attempts to prepare the organic soluble CB[8]•**11**•2PF_6 complex were not successful according to ^{1}H NMR analysis.

Molecular modelling of self-assembled tetrahedra 12 and 13

We performed molecular modelling of tetrahedra **12** and its analogue fully interlocked with six CB[7] rings **12**•CB[7]$_6$. Figure 5(a,b) shows the structures of **12** and **12**•CB[7]$_6$ minimised by molecular mechanics using the MMFF94s force field implemented within the Spartan '16 software package. As can be seen, **12** features a roughly tetrahedral geometry with a large central cavity. The average distance between Fe atoms of MOP **12** is 24.9 Å and the distance from the centroid of the four Fe atoms to the outside edge of the MOP is 19.1 Å. Accordingly, the rough diameter of the MMFF94s minimzed structure of **12** is 38.2 Å which is slightly smaller than the hydrodynamic diameter (41.4 Å) calculated from the DOSY data. The hydrodynamic diameter of **12** in solution also reflects the contributions of the 20 PF_6 counterions so this small difference is not surprising. It should be noted that the edges of **12** are slightly bowed outward in the molecular model which is likely due to electrostatic repulsion between dicationic viologen units in the overall 20+ assembly. Figure 5(b) shows the MMFF94s minimised structure of **12**•CB[7]$_6$ which is roughly tetrahedral with average iron-iron distances of 25.0 Å and centroid to iron distance of 15.3 Å. The structure calculated structure easily accommodates six CB[7] units and there is no evidence of close contacts or even van der Waals interactions between CB[7] units in the minimised structure of **12**•CB[7]$_6$. Accordingly, the experimental observation that assembly **13** contains 1.8 CB[7] units on average must be due to other factors including the poor solubility of CB[7] in the reaction mixture and the potential for repulsive electrostatic interactions between the electrostatically negative convex outer surfaces of CB[7] units [34]. The distance between the centroid of the iron atoms of **12**•CB[7]$_6$ and the outer edge of the ligands is 19.3 Å which corresponds to a calculated diameter of 38.6 Å. This calculated value for **12**•CB[7]$_6$ is very similar to the value measured for **13**•20PF_6 by DOSY (Table 1).

Synthesis of isomeric bipyridine ligand 16 and self-assembly to give cubic MOP 17

Although we were pleased that cage **12** could be threaded to give cage **13** containing an average of two CB[7] units, we were disappointed that full occupancy of the edges (e.g. six CB[7]) could not be achieved. We decided to create a larger self-assembly that would have a larger central cavity that might be able to better accommodate a larger number of CB[n] rings. We realised that ligand **16** (Scheme 6) – which is a constitutional isomer of **11** – possesses a geometry [107] that should deliver a self-assembled cube upon reaction with Fe(II) salts. For the synthesis of **16**, we first performed the Suzuki coupling reaction between commercially available 4-bromo-2,2′-bipyridine **14** and

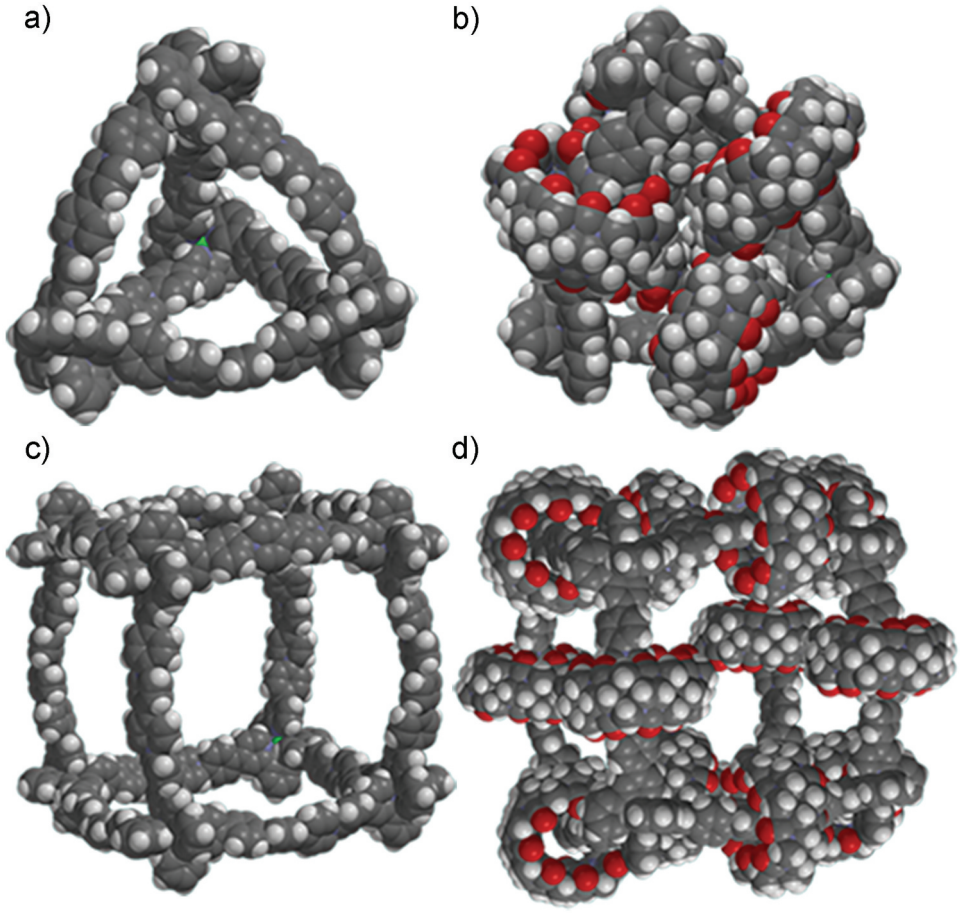

Figure 5. A) Molecular modelling of (a) **12**, (b) **12**•6CB[7], (c) **17**, and (d) **17**•12CB[7] .

9 using $Pd(PPh_3)_4$ as catalyst to deliver **15** in 64% yield. Subsequently, the Zincke reaction [91] between **15** and **1** was performed in refluxing EtOH to deliver **16** in 77% yield. Compound **16** was fully characterised by the standard spectroscopic methods. For example, characteristic ^{1}H NMR resonances for the viologen aromatic protons (H_j and H_k) appear at 9.52 ppm and 8.86 ppm (Supporting Information, Figure S71) whereas a pair of aromatic doublets appear at 8.23 ppm and 8.04 ppm for the phenylene linker (H_i and H_h) along with seven additional aromatic resonances (H_a – H_g) are for the bipyridyl end group (triplets for H_a and H_b, a singlet for H_g, and three doublets for H_d – H_f. The ^{13}C NMR spectrum for **16** recorded in DMSO-d_6 (Supporting Information, Figure S72) displays 17 resonances in the aromatic region of the spectrum which is consistent with the C_{2v}-symmetric structure depicted in Scheme 6.

Given our previous success in the self-assembly of **12** in acetonitrile, we first converted **16** into the corresponding organic soluble PF_6 and NTf_2 salts. To prepare self-assembled cube **17** we heated a 12:8 mixture of **16**•2PF_6 (or **16**•2NTf_2) with $Fe(OTf)_2$ (or $Fe(NTf_2)_2$) in acetonitrile at 60 °C for 24 hours (Scheme 7). During the course of the reaction the colour changes from orange-brown to deep purple. The UV/Vis spectra recorded for **16** and **17** is given in the Supporting Information (Figure S94). The spectrum for **17** shows a new λ_{max} at 544 nm which is comparable to that observed for **12** (λ_{max} = 539 nm) which provides strong support for the formation of the iron(bipyridine)$_3$ corners. The ^{1}H NMR spectrum recorded for **17** in CD_3CN is shown in Figure 6. The assignments of the resonances to specific protons in Figure 6 are based on the correlations observed in the COSY spectrum of **17** (Supporting Information, Figure S88). Most significantly, the protons adjacent to the bipyridine N-atoms undergo substantial upfield changes in chemical shift upon transformation of **16** to **17** (H_c: 8.83 to 7.62 ppm; H_g: 8.73 to 7.53 ppm). These large upfield shifts reflect the fact that these protons are located in the anisotropic shielding region of the adjacent bipyridine within assembly **17** as was also seen for **12**. Bipyridine protons H_b (7.96 to 8.24 ppm), H_d (8.51 to 8.84 ppm), and H_e (8.70 to 8.96 ppm) undergo slight downfield shifts upon formation of **17** which is reflective of the change in electronics of the bipyridine ring upon coordination to Fe^{II}. To gain insight into the

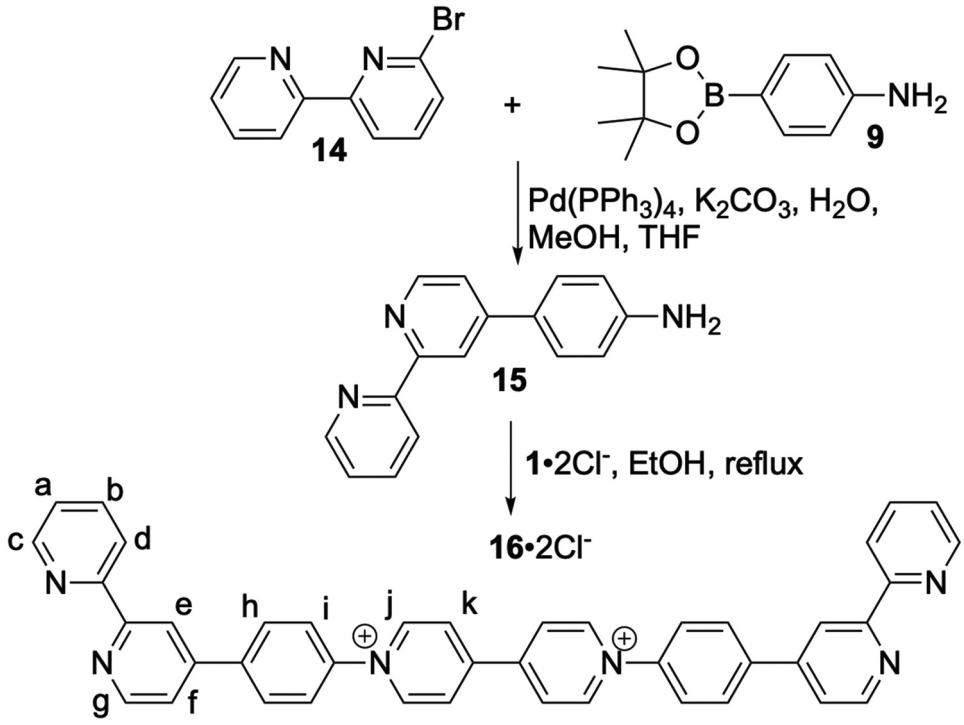

Scheme 6. Synthesis of isomeric bipyridine ligand **16.**

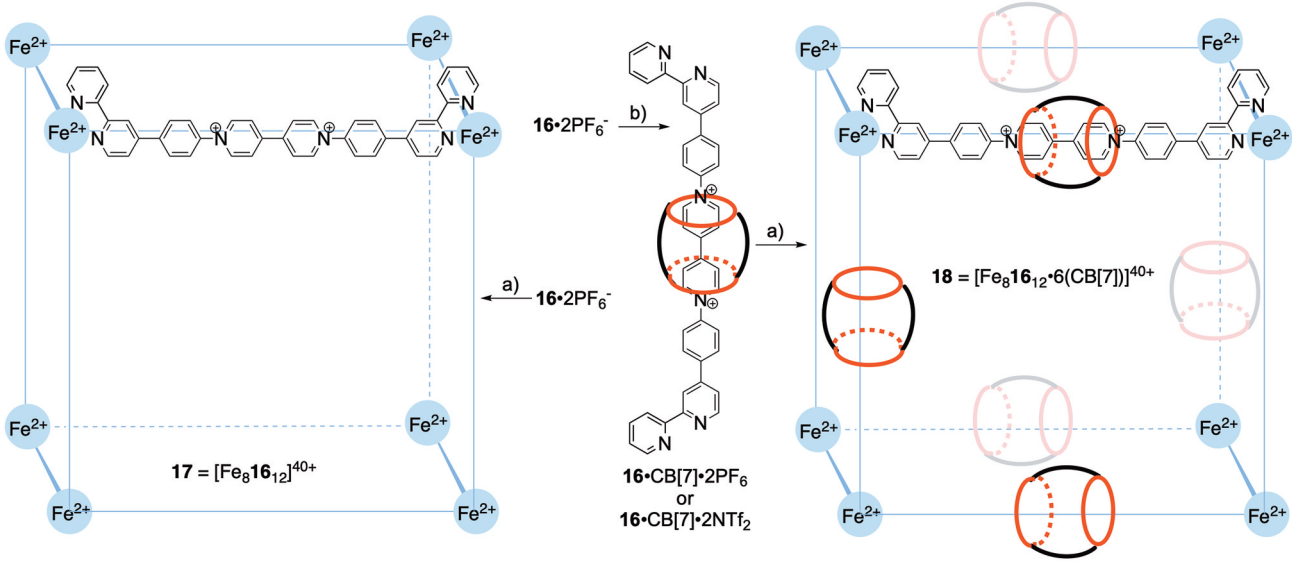

Scheme 7. Self-assembly of MOPs **17** and **18**. Conditions: (a) $Fe(OTf)_2$, CH_3CN, (b) D_2O, CB[7], then NH_4PF_6.

size of assembly **17** we performed DOSY NMR in CD_3CN at 298 K that allowed us to calculate the diffusion coefficient for **17** (D = 1.40 x 10^{-10} m/s^2) and its hydrodynamic diameter (91.3 Å). Cage **17** diffuses 5.51 times slower than ligand **16** (D = 7.71 x 10^{-10} m/s^2) and 2.20 times slower than tetrahedron **12**. Figure 5(c) shows the structure of an MMFF94S minimised model of **17** which is roughly cubic with an edge length of 27.7 Å. The maximum distance from the centroid of the eight iron atoms to the outer edges of **17** is 28.1 Å which corresponds to a diameter of 56.2 Å. The calculated diameter of **17** and the hydrodynamic diameter of **17** measured in solution differ in part because of the influence of the 40 PF_6 counterions and perhaps also due to the effects of aggregation [96]. Overall, the confluence of the data provides significant evidence for the formulation of the structure of **17** as a cubic assembly. Unfortunately, despite numerous attempts we were not able to observe

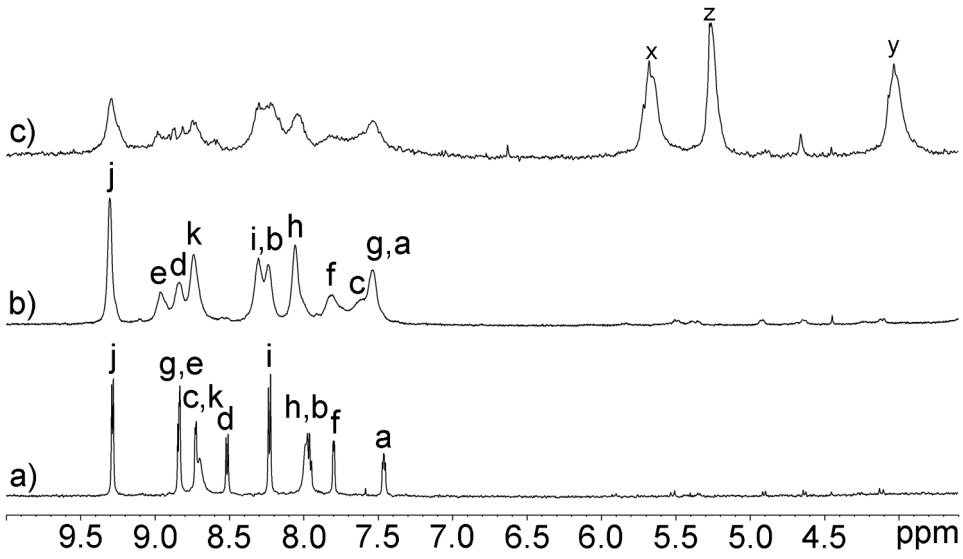

Figure 6. ^{1}H NMR spectra recorded (600 MHz, CD_3CN, RT) for: (a) **16**•2PF_6, (b) **17**•20PF_6, and (c) **18**•40NTf_2.

ions in the ESI-MS spectrum for either **17**•40PF_6 or **17**•40NTf_2 that could be assigned to the depicted cubic assembly.

Mechanical interlocking of CB[7] onto the edges of cage 17 to give cage 18

Next, we set out to mechanically interlock CB[7] units onto the edges of self-assembled cube **17**. Initially, we tested the complexation of an equimolar mixture of CB[7] with **16**•2Cl in D_2O by ^{1}H NMR (Supporting Information, Figure S79). We observe upfield shifting for phenylene protons H_h (8.05 to 7.14 ppm) and H_i (8.25 to 7.34 ppm) and viologen proton H_j (9.53 to 9.10 ppm) and downfield shifting of viologen proton H_k (8.88 to 8.98 ppm) upon complexation with CB[7]. This data indicates that the primary binding site is the phenylene unit. Accordingly, we decided to follow the strategy employed for the assembly of **13** involving CH_3CN soluble salts. Experimentally, we treated aqueous solutions of CB[7]•**16**•2Cl with excess $LiNTf_2$ and separately with excess NH_4PF_6 which gave CB[7]•**16**•2NTf_2 and CB[7]•**16**•2PF_6 as precipitates that could be isolated by centrifugation, washing with water, and drying under high vacuum (Scheme 7). For the self-assembly reaction, we heated equimolar mixtures of CB[7]•**16**•2NTf_2 (or CB[7]•**16**•2PF_6) and $Fe(NTf_2)_2$ (or $Fe(OTf)_2$) at 60 °C in acetonitrile for 24 hours to give **18**. The reaction mixture rapidly assumes a deep purple colour. Assembly **18** can be isolated by precipitation from the reaction mixture by addition of Et_2O followed by centrifugation, decantation, and drying. Figure 6(c) shows the ^{1}H NMR spectrum recorded for **18** in CD_3CN which is broadened and unfortunately the multiplicity cannot be observed for individual resonances. The broadness of the ^{1}H NMR spectrum rendered the COSY spectrum of no value. However, a comparison of the aromatic regions of Figure 6(b,c) make it clear that very similar assemblies are formed in both cases. Furthermore, integration of the resonances for the CB[7] units (H_x, H_y, H_z) versus those of ligand **16** allow us to determine that assembly **18** contains an average of 6.59 molecules of CB[7]. We acquired the DOSY spectrum for **18** in acetonitrile which established that the CB[7] units of the assembly diffuse at the same rate as aromatic units of the assembly which provides strong evidence for the mechanical interlocking of the CB[7] units onto the edges of the assembly. Figure 5(d) shows an MMFF94s minimised model of **17**•(CB[7])12 which does not show any steric interactions between the adjacent CB[7] units. The observation that assembly **18** contains an average of 6.59 CB[7] units must be due to other factors including the poor solubility of CB[7] in the reaction medium or perhaps unfavourable electrostatic interactions between the electrostatically positive convex faces of the CB[7] units. The DOSY spectrum allowed us to calculate the diffusion coefficient for **18** ($D = 1.25 \times 10^{-10}$ m/s^2) along with its hydrodynamic diameter (102 Å). The hydrodynamic diameter of **18** is very similar to that of **17** (91.3 Å) which provides further support for the formulation of both **17** and **18** as cubes. Overall, the data provides clear evidence

for the incorporation of multiple CB[7] units onto the edges of assembly **18** but, unfortunately, even with this larger cubic system it was not possible to achieve full occupation of all 12 edges with CB[7] units.

Conclusions

In summary, we have reported our initial investigations into the preparation of MOPs that contain mechanically interlocked CB[n] units as a precursor to using the molecular recognition properties of such assemblies for drug delivery purposes. Initially, we prepared dianiline ligand **4**•2Cl – which contains a central viologen unit as a CB[n] binding site – and performed self-assembly with pyridine-2-carboxaldehyde and $Fe(OTf)_2$ in acetonitrile and observed the formation of a single species by ^{1}H and DOSY NMR that we assign as tetrahedron **6**. When the organic soluble CB[7]•**11**•2PF_6 complex was self-assembled with $Fe(OTf)_2$ in acetonitrile, assembly **7** with an average of 1.95 mechanically interlocked CB[7] units was obtained. Unfortunately, MOPs **6** and **7** were hydrolytically unstable in water and therefore are not appropriate for drug delivery studies. Accordingly, analogous organic soluble ligands **11**•2(NTf_2) and **16**•2PF6 that feature terminal 2,2′-bipyridine groups were prepared and their self-assembly with $Fe(NTf_2)_2$ or Fe(OTf) was performed which delivered tetrahedral assembly **12** and cubic assembly **17** as evidenced by analysis of complexation induced changes in ^{1}H NMR chemical shift, DOSY, and ESI-MS results for **12**. Assemblies **12** and **17** are stable under aqueous conditions. Finally, threading of ligands **11** and **16** with CB[7] gave the acetonitrile soluble complexes CB[7]•**11**•2PF_6 and CB[7]•**16**•2PF_6 which underwent assembly with $Fe(OTf)_2$ in acetonitrile to give self assembled tetrahedron **13** and cube **18** which on average contain 1.80 and 6.59 CB[7] molecules, respectively. In conclusion, we find that the self-assembly of MOPs with mechanically interlocked CB[7] requires that the CB[7] units reside on the viologen unit which is favoured in acetonitrile rather than the phenylene binding epitope. Our inability to achieve full binding of CB[7] to every MOP edge cannot be ascribed to steric effects but probably reflects partial dissociation of the CB[7]•**11** or CB[7]•**16** complexes under the reaction conditions. Future work targets new ligands with tighter binding and slower dissociating CB[n] binding domains that may assemble to give MOPs fully saturated with mechanically interlocked CB[n].

Experimental details

Compounds **1** [89], **2** [90], and **10** [102] were prepared according to literature procedures. NMR spectra were measured on 400 MHz, 500 MHz, and 600 MHz spectrometers (400, 500, 600 MHz for ^{1}H NMR; 100, 126 MHz for ^{13}C NMR) at room temperature in the stated deuterated solvents unless otherwise stated. Low resolution mass spectrometry was performed using a JEOL AccuTOF electrospray instrument. Electrospray ionisation-mass spectrometry (ESI-MS) for cage samples was performed on a Waters Synapt G2 mass spectrometer, using sample solutions (1 mg mL^{-1}) in DMSO/CH_3CN (1/1, v/v). The ESI-MS experiments were carried out under the following conditions: ESI capillary voltage, 3 kV; sample cone voltage, 30 V; extraction cone voltage, 0.1 V; source temperature 100°C; desolvation temperature, 100°C; cone gas flow, 10 L/h; desolvation gas flow, 700 L/h (N_2).

Compound 3 (Chloride salt)

Compound **1** (0.437 g, 0.778 mmol) was dissolved in EtOH (75.0 mL) and then **2** (0.446 g, 1.57 mmol) was added to the reaction flask causing the yellow solution to turn dark brown. The reaction mixture was stirred and heated at reflux overnight. The reaction mixture was allowed to cool to room temperature and then the majority of the solvent (20 mL remaining) was removed by rotary evaporation. The heterogenous mixture was then poured into THF (800 mL) and stirred at room temperature for 2 h which resulted in a brown precipitate. The solid was collected by filtration to afford **3** as a dark red powder (569 mg, 96% yield). M.p. > 300°C. IR (ATR, cm^{-1}) 3359 m, 3030 m, 1702 m, 1630 m, 1584 m, 1529 m, 1489 m, 1367 m, 1319 m, 1234 m, 1152s, 1053 m, 818s. ^{1}H NMR (600 MHz, DMSO-d_6): 9.73 (d, J = 6.0 Hz, 4H), 9.57 (s, 2H), 9.09 (d, J = 6.0 Hz, 4H), 8.05 (d, J = 8.4 Hz, 4H), 8.03 (d, J = 8.4 Hz, 4H), 7.77 (d, J = 8.3 Hz, 4H), 7.64 (d, J = 8.3 Hz, 4H), 1.50 (s, 18 H). ^{13}C NMR (126 MHz, DMSO-d_6): 152.8, 148.8, 145.7, 142.9, 140.7, 140.2, 131.4, 127.5, 127.4, 126.7, 125.3, 118.6, 79.4, 20.1. ESI-MS (ESI): *m/z* 346.3 ($[M]^{2+}$), calcd. for $C_{44}H_{44}N_4O_4$, 346.4.

Compound 4 (Chloride salt)

Compound **3** (0.301 g, 0.395 mmol) was suspended in CH_2Cl_2 (30 mL) and the slurry was cooled in an ice-water bath. TFA (6.0 mL) was added dropwise over 30 minutes which resulted in a red solution. The solution was removed from the ice bath and stirred at room temperature for 2 hours. The solvent was removed by rotary evaporation yielding a dark yellow oil. The oil was treated with EtOH (10 mL) and then the solvent was removed by rotary evaporation which resulted in a purple gummy solid. Repetition of the treatment with

EtOH two more times ultimately gave **4** as the dichloride salt as a dark yellow solid (0.367 g, 98%) after drying on high vacuum overnight. M.p. > 300°C. IR (ATR, cm^{-1}) 3400 w, 2920 w, 2851 w, 1631 m, 1608 m, 1592 m, 1492 m, 1285 w, 1199 w, 824s. ^{1}H NMR (600 MHz, D_2O): 9.43 (d, *J* = 6.9 Hz 4H), 8.78 (d, *J* = 6.9 Hz, 4H), 7.97 (d, *J* = 8.6 Hz, 4H), 7.87 (d, *J* = 8.6 Hz, 4H), 7.66 (d, *J* = 8.4 Hz, 4H), 6.98 (d, *J* = 8.4 Hz, 4H). ^{13}C NMR (100 MHz, D_2O, Dioxane as reference): 150.6, 145.4, 143.1, 141.8, 129.2, 129.0, 127.2, 124.7, 123.5. ESI-MS (ESI, sample dissolved in H_2O): *m/z* 246.1 ($[M]^{2+}$), $C_{34}H_{28}N_4$, calculated 246.3.

Compound 4 (Hexafluorophosphate salt)

First, counter anion exchange from chloride to hexafluorophosphate was performed by dissolving **4** (9.1 mg, 11.5 µmol) in water (5.0 mL) and then adding NH_4PF_6 (22.3 mg, 115 µmol) which caused a purple precipitate to form. The heterogenous mixture was sonicated for 30 minutes. The solid was obtained by centrifugation and the pellet was suspended in water (2.0 mL) with the help of vortexing and sonication and then the mixture was centrifuged. The supernatant was decanted. The process was repeated 3 times to ensure excess NH_4PF_6 was removed followed by drying under high vacuum to give **4** (hexafluorophosphate salt, 7.1 mg, 9.1 µmol, 79%). M.p. > 300°C. IR (ATR, cm^{-1}) 3076 m, 2833 m, 2600 m, 1740s, 1679s, 1634 m, 1545 w, 1520 w, 1492 m, 1433 w, 1406 w, 1224 w, 1196s, 1131s, 1005 w, 862 w, 832 w, 817 m, 805 m, 790 m, 720 m, 666 m. ^{1}H NMR (600 MHz, CD_3CN): 9.22 (d, *J* = 7.08 Hz, 4H), 8.65 (d, *J* = 7.08 Hz, 4H), 7.95 (d, *J* = 8.81 Hz, 4H), 7.80 (d, *J* = 8.81 Hz, 4H), 7.56 (d, *J* = 8.61 Hz, 4H), 6.79 (d, *J* = 8.61 Hz, 4H). ^{13}C NMR (126 MHz, DMSO-d_6): 149.7, 148.5, 145.4, 143.8, 139.6, 127.7, 126.5, 126.4, 125.0, 124.6, 114.2. ESI-MS (ESI, sample dissolved in CH_3CN): *m/z* 246.2 ($[M]^{2+}$), $C_{34}H_{28}N_4$, calculated 246.3.

Compound 4 (Triflimide salt)

First, counter anion exchange from chloride to triflimide was performed by dissolving **4** (11.6 mg, 12.3 µmol) in water (2.0 mL) and then adding $LiNTf_2$ (291 mg, 1.01 mmol) which caused a purple precipitate to form. Heterogenous mixture was sonicated for 30 minutes. The solid was obtained by centrifugation and the pellet was suspended in water (2.0 mL) with the help of vortexing and sonication and then the mixture was centrifuged. The supernatant was decanted. The process was repeated 3 times to ensure excess $LiNTf_2$ was removed followed by drying under high vacuum to give **4** (triflimide salt, 10.7 mg, 10.2 µmol, 83%). M.p. > 300°C. IR (ATR, cm^{-1}) 3648 w, 3401 w, 3126 w, 2919 m, 2851 w, 2362 w, 1632 m, 1609 m, 1593 m, 1530 w, 1492 m, 1435 w, 1410 w, 1285 w, 1199 w, 1003 w, 815s, 740 w. ^{1}H NMR (400 MHz, CD_3CN): 9.22 (d, *J* = 7.1 Hz, 4H), 8.65 (d, *J* = 7.1, Hz, 4H), 7.95 (d, *J* = 8.9, Hz, 4H), 7.80 (d, *J* = 8.9, Hz, 4H), 7.56 (d, *J* = 8.6 Hz, 4H), 6.79 (d, *J* = 8.6 Hz, 4H), 4.48 (br. s, 4H). ^{13}C NMR (126 MHz, CD_3CN): 150.8, 150.2, 146.3, 146.0, 141.0, 129.2, 128.5, 128.3, 127.5, 125.8, 115.8. ESI-MS (ESI, sample dissolved in CH_3CN): *m/z* 246.1 ($[M]^{2+}$), $C_{34}H_{28}N_4$, calculated 246.3.

Cage 6 (Hexafluorophosphate salt)

Hexafluorophosphate salt **4** (10.4 mg, 13.3 µmol) and iron (II) triflate (3.1 mg, 8.8 µmol) were placed in a scintillation vial with a stir bar and capped with a rubber septum. The vial was purged of oxygen by several cycles of high vacuum and then refilling with N_2 gas. Subsequently, **5** (2.5 µL, 26 µmol) and dry acetonitrile (0.9 mL) were added by syringe. The reaction vial was sonicated for 30 minutes which resulted in a dark purple solution. The reaction mixture was then stirred at 60°C for 24 h. After cooling to room temperature, Et_2O (6.0 mL) was added to the reaction mixture which caused **6** to precipitate. After centrifugation and decantation of the supernatant, **6** was obtained as a purple solid. Purple solid was redissolved in CH_3CN (0.5 mL) and excess NH_4PF_6 (4.4 mg, 27 µmol) was added. Et_2O (6.0 mL) was added to the solution causing **6** to precipitate. After centrifugation and decantation of the supernatant, **6**•$20PF_6$ was air dried and obtained as a purple solid (9.3 mg, 90%). IR (ATR, cm^{-1}): 3125 w, 3070w, 1633 m, 1595 w, 1488 m, 1443 w, 1400 w, 1254 m, 1223 m, 1160 m, 1028 m, 1005 w, 816s, 774 m, 750 w, 740 w. ^{1}H NMR (400 MHz, CD_3CN): 9.24 (br. s, 24 H), 8.95–8.90 (m, 12 H), 8.68 (br. s, 24 H), 8.58 (br. d, 12 H), 8.44 (br. t, 12 H), 8.09 (br. s, 24 H), 7.93 (br. s, 24 H), 7.82 (br. t, 12 H), 7.70–7.65 (m, 24 H), 7.50–7.45 (m, 12 H), 5.60–5.55 (m, 24 H). ^{13}C NMR (126 MHz, CD_3CN): 175.9, 159.2, 157.1, 151.6, 151.5, 146.8, 144.0, 143.1, 140.9, 140.0, 132.6, 131.3, 130.3, 129.7, 128.7, 128.6, 126.3, 123.3.

Cage 6 (Triflimide salt)

Triflimide salt **4** (5.7 mg, 5.4 µmol) was placed in a scintillation vial with a stir bar and iron (II) triflimide (2.6 mg, 4.2 µmol) and capped with a rubber septum. The vial was purged of oxygen by several cycles of high vacuum and then refilling with N_2 gas. Subsequently, dry acetonitrile (1.0 mL) and **5** (0.5 µL, 5 µmol) was added by syringe. The reaction vial was sonicated for 30 minutes which resulted in a dark purple solution. The reaction

mixture was then stirred at 60°C for 24 h. After cooling to room temperature, Et_2O (6.0 mL) was added to the reaction mixture which caused **6** to precipitate. After centrifugation and decantation of the supernatant, **6** was obtained as a purple solid which was air dried. ^{1}H NMR (600 MHz, CD_3CN): 9.24 (br. s, 24 H), 9.00–8.95 (m, 12 H), 8.69 (br. m, 24 H), 8.65–8.55 (br. m, 12 H), 8.50–8.40 (br. m, 12 H), 8.06 (d, J = 8.6 Hz, 24 H), 7.93 (br. m, 24 H), 7.83 (br. m, 12 H), 7.75–7.60 (m, 24 H), 7.55–7.45 (m, 12 H), 5.70–5.60 (m, 24 H). ^{13}C NMR (126 MHz, CD_3CN): 175.9, 157.1, 151.7, 151.5, 151.4, 146.6, 144.0, 143.0, 140.9, 140.0, 132.5, 131.3, 130.1, 129.5, 128.49, 128.43, 126.2, 126.0, 125.4, 124.1, 123.3, 122.0, 119.9.

Cage 7 (Hexafluorophosphate salt)

Solid CB[7] (3.0 mg, 2.6 µmol) and **4**•2Cl (2.4 mg, 2.5 µmol) was dissolved in D_2O (1.0 mL). The 1:1 stoichiometric ratio was confirmed by ^{1}H NMR integration of the resonances of CB[7] versus **4**. An excess of NH_4PF_6 (7.7 mg, 47 µmol) was added to the solution causing a dark brown solid to precipitate. The heterogenous mixture was sonicated for 30 minutes before being centrifuged and the supernatant was decanted. The moist solid was suspended in water with the help of sonication followed by centrifugation. The brown solid was dried on high vacuum overnight to give **4•CB[7]** (4.6 mg, 90%). Solid **4**•CB[7] (2.3 mg, 1.2 µmol) was placed in a scintillation vial with a stir bar and capped with a rubber septum. The vial was purged of oxygen by several cycles of high vacuum and then refilling with N_2 gas. Subsequently, **5** (0.2 µL, 2 µmol), a solution of iron (II) triflate (16 mM, 50 µL, 0.8 µmol) in dry acetonitrile, and dry acetonitrile (50 µL) was added by syringe. The reaction vial was sonicated for 30 minutes which gave a dark purple solution. The reaction was then stirred at 60°C for 24 h. The reaction mixture was cooled to room temperature and then Et_2O (6.0 mL) was added which resulted in a precipitate. The heterogenous mixture was centrifuged, the supernatant removed, and the pellet was dried in air to give **7** as a purple solid. Purple solid was redissolved in CH_3CN (0.5 mL) and excess NH_4PF_6 (2.0 mg, 12 µmol) was added. Et_2O (6.0 mL) was added to the solution causing **7** to precipitate. After centrifugation and decantation of the supernatant, **7**•20PF_6 was air dried and obtained as a purple solid (1.9 mg, 56%). IR (ATR, cm^{-1}): 3366 w, 3124 w, 1738s, 11,632 m, 1595 w, 1488 m, 1464s, 1423 m, 1375 m, 1320 m, 1278 m, 1227s, 1189s, 1029 m, 1005 w, 968 m, 830s, 800s, 756 m, 672 w. ^{1}H NMR (600 MHz, CD_3CN, RT): 9.26–9.18 (m, 24 H), 8.97 (br. m, 12 H), 8.70–8.60 (m, 28 H), 8.45 (br., 12 H), 8.25–8.20 (m, 16 H), 8.10 (br., 18 H), 7.94 (br., 18 H), 7.82 (br., 16 H), 7.69 (br., 24 H), 7.47 (br., 12 H), 7.11 (br., 8H), 5.67–5.58 (m, 52H), 5.27 (s, 28 H), 4.06 (d, J = 13.0 Hz, 28 H). ^{13}C NMR (126 MHz, CD_3CN): 190.3, 175.8, 159.2, 157.1, 156.3, 151.5, 148.9, 146.7, 144.0, 143.0, 142.8, 140.9, 140.0, 138.8, 132.5, 131.3, 130.3, 130.1, 129.6, 138.5, 128.1, 126.2, 126.0, 124.1, 123.2, 71.7, 53.4.

Cage 7 (Triflimide salt)

Solid CB[7] (6.2 mg, 5.3 µmol) and **4** (5.6 mg, 5.9 mmol) was dissolved in D_2O (2.0 mL). The 1:1 stoichiometric ratio was confirmed by ^{1}H NMR integration of the resonances of CB[7] versus **4**. An excess of $LiNTf_2$ (169 mg, 0.655 mmol) was added to the solution causing a dark brown solid to precipitate. The heterogenous mixture was sonicated for 30 minutes before being centrifuged and the supernatant was decanted. The moist solid was suspended in water with the help of sonication followed by centrifugation. The brown solid was dried on high vacuum overnight to give **4**•CB[7] (12.3 mg, 94%). Solid **4**•CB[7] (6.1 mg, 2.8 µmol) was placed in a vial with a stir bar and iron (II) triflimide (1.3 mg, 2.1 µmol). The vial was capped with a rubber septum and deoxygenated by repeated cycles of high vacuum and then refilling with N_2 gas. Dry acetonitrile (0.6 mL) and **5** (0.3 µL, 3 µmol) were added by syringe. The reaction vial was sonicated for 30 minutes which gave a dark purple solution. The reaction was then stirred at 60°C for 24 h. The reaction mixture was cooled to room temperature and then Et_2O (6.0 mL) was added which resulted in a precipitate. The heterogenous mixture was centrifuged, the supernatant removed, and the pellet was dried in air to give **7** as a purple solid. ^{1}H NMR (600 MHz, CD_3CN, RT): 9.25–9.15 (m), 8.90 (br. m), 8.70 (br. s), 8.25–7.80 (m), 7.70–7.65 (m), 7.46 (br. s), 7.40–7.25 (m), 7.14 (br. s), 5.70 (d), 5.27 (br. s), 4.06 (d). ^{13}C (126 MHz, CD_3CN, RT): 156.3, 151.9, 148.9, 146.7, 131.4, 130.9, 130.4, 130.1, 128.3, 128.1, 128.0, 127.5, 127.3, 126.3, 126.1, 124.5, 124.2, 124.0, 122.0, 120.3, 119.9, 71.6, 53.4.

Compound 11 (Chloride salt)

Compound **1** (0.205 g, 0.827 mmol) and **10** (0.211 mg, 0.376 mmol) were dissolved in EtOH (55.0 mL). The solution was heated at reflux for 24 h during which the solution turned brown in colour. The reaction was then concentrated by rotary evaporation (to ≈ 20 mL) and then poured into THF (500 mL). After stirring for 2 hours at room temperature, a yellow precipitate was observed which was isolated by filtration. The crude solid was washed on the frit with THF (10 mL) three times to afford **11** as the chloride salt (259 mg, 97%). M.p. > 300°C. IR

(ATR, cm^{-1}): 3368 m, 3107 w, 1628s, 1587 m, 1460s, 1433s, 1417 m, 1368 m, 1342 w, 1244 m, 1093 w, 1072 w, 1034 w, 1000s, 832s, 817s. ^{1}H NMR (600 MHz, DMSO-d_6, RT): 9.80 (d, J = 6.4 Hz, 4H), 9.21 (s, 2H), 9.14 (d, J = 6.4 Hz, 4H), 8.76 (d, J = 6.5 Hz, 2H), 8.58 (d, J = 8.2 Hz, 2H), 8.48 (d, J = 6.5 Hz, 2H), 8.45 (d, J = 8.2 Hz, 2H), 8.30 (d, J = 8.3 Hz, 4H), 8.17 (d, J = 8.3 Hz, 4H), 8.02 (t, J = 6.5 Hz, 2H), 7.52 (t, J = 6.5 Hz, 2H). ^{13}C NMR (126 MHz, DMSO-d_6): 155.1, 154.2, 149.4, 149.0, 147.7, 145.9, 139.9, 139.6 137.6, 135.7, 134.4, 128.5, 126.6, 125.7, 125.1 120.6. ESI-MS (ESI, sample dissolved in H_2O): m/z 309.1 ($[M]^{2+}$), $C_{42}H_{30}N_6$, calculated 309.4.

Compound 11 (Hexafluorophosphate salt)

Compound **11** (chloride) was transformed into the hexafluorophosphate salt by dissolving **11** · 2Cl (36.8 mg, 53.4 µmol) in water (12 mL) and heating to 80°C followed by the addition of NH_4PF_6 (90.7 mg, 556 mmol) was resulted in the formation of a precipitate. Heterogenous mixture was stirred at 80°C for 30 minutes. The heterogenous mixture was cooled to room temperature, centrifuged, and the supernatant was decanted to give a moist solid. The moist solid was suspended in water (2.0 mL) with the help of sonication, followed by centrifugation, and removal of the supernatant. This process was repeated three times to remove excess NH_4PF_6 and then the solid **11**•2PF_6 was dried under high vacuum (39.1 mg, 81%). M.p. > 300°C. IR (ATR, cm^{-1}): 3135 w, 3053 w, 2924s, 2362 w, 1636 m, 1588 m, 1552 w, 1485 w, 1458 m, 1435 m, 1417 w, 1369 w, 1264 w, 1216 w, 1149 w, 1094 w, 1067 w, 1043 w, 1002 w, 877s, 794 m, 752w, 741 w, 716w, 695 w. ^{1}H NMR (600 MHz, CD_3CN, RT): 9.29 (d, J = 7.0, 4H), 9.10 (d, J = 4.1 Hz, 2H), 8.75–8.70 (m, 6H), 8.61 (d, J = 9.5 Hz, 2H), 8.50 (d, J = 7.9, 2H), 8.29 (dd, J = 4.1, 9.5 Hz, 2H), 8.17 (d, J = 8.7 Hz, 4H), 8.00–1.90 (m, 6H), 7.45 (t, J = 4.8 Hz, 2H). ^{13}C NMR (126 MHz, CD_3CN): 150.4, 148.9, 146.7, 143.0, 138.7, 137.3, 136.9, 130.2, 128.4, 126.3, 125.3, 121.9. ESI-MS (ESI, sample dissolved in CH_3CN): m/z 309.0 ($[M]^{2+}$), $C_{42}H_{30}N_6$, calculated 309.4.

Compound 11 (Triflimide salt)

Compound **11** (chloride) was transformed into the triflimide salt by dissolving **11** · 2Cl (23.9 mg, 34.7 µmol) in water (10 mL) and heating to 80°C followed by the addition of $LiNTf_2$ (107.2 mg, 373 µmol) was resulted in the formation of a precipitate. Heterogenous mixture was stirred at 80°C for 30 minutes. The heterogenous mixture was cooled to room temperature, centrifuged, and the supernatant was decanted to give a moist solid. The moist solid was suspended in water (4.0 mL) with the help of sonication, followed by centrifugation, and removal of the supernatant. This process was repeated three times to remove excess LiNTf2 and then the solid **11** (29.2 mg, 71%) was dried under high vacuum. M.p. > 300°C. IR (ATR, cm^{-1}): 3124 w, 3068 w, 1632 m, 1587 w, 1573 w, 1550 w, 1485 w, 1458 m, 1436 w, 1419 w, 1351s, 1331s, 1179s, 1129s, 1093 w, 1050s, 1000 m, 877 w, 828 m, 799 m, 756 m, 739 m. ^{1}H NMR (400 MHz, CD_3CN, RT): 9.29 (d, J = 6.7, 4H), 9.10 (d, J = 2.1 Hz, 2H), 8.75–8.70 (m, 6H), 8.61 (d, J = 8.3 Hz, 2H), 8.50 (d, J = 7.9, 2H), 8.29 (dd, J = 2.1, 8.3 Hz, 2H), 8.17 (d, J = 8.6 Hz, 4H), 8.00–1.90 (m, 6H), 7.45 (t, J = 5.1 Hz, 2H). ^{13}C NMR (126 MHz, DMSO-d_6): 155.1, 154.6, 149.5, 149.0, 147.7, 145.9, 141.9, 139.9, 137.5, 135.7, 133.7, 128.5, 126.6, 125.7, 124.5, 120.6, 118.4. ESI-MS (ESI, sample dissolved in CH_3CN): m/z 309.0 ($[M]^{2+}$), $C_{42}H_{30}N_6$, calculated 309.4.

Cage 12 (Hexafluorophosphate salt)

A solution of iron (II) triflate (10.7 mM, 0.5 mL, 5.37 µmol) in CH_3CN was added to a vial with solid hexafluorophosphate salt **12** (5.7 mg, 6.27 µmol) suspended in CH_3CN (1.0 mL). Once iron was added, the yellow suspension turned ruby red. The mixture was sonicated for 30 minutes and then stirred at 60°C for 24 h resulting in a ruby red homogenous solution. The red solution was cooled to room temperature and then Et_2O (6.5 mL) was added which resulted in a red solid. The heterogenous mixture was centrifuged followed by removal of the supernatant. The solid was resuspended in Et_2O (6.0 mL) with the help of sonication followed by centrifugation and decantation of the supernatant to obtain the red solid. The process was repeated two more times. Red solid was then redissolved in a solution of NH_4PF_6 (77 mM, 0.25 mL, 3.1 mmol) in CH_3CN. Et_2O (5.0 mL) was added causing **12** to precipitate. Red solid was collected by centrifugation and decantation. The solid was resuspended in Et_2O (6.0 mL) with the help of sonication followed by centrifugation and decantation of the supernatant to obtain the red solid. The process was repeated two more times. Cage **12**•20PF_6 was air dried and obtained as a red solid (4.3 mg, 60%). IR (ATR, cm^{-1}): 3657 w, 3587 w, 3129 w, 2360 w, 1634 m, 1605 w, 1490 w, 1467 m, 1440 m, 1377 w, 1344 w, 1243 w, 1168 w, 1010 w, 1008 w, 815s, 752 m, 738 m. ^{1}H NMR (600 MHz, CD_3CN, RT): 9.15 (d, J = 5.9 Hz, 24 H), 8.74 (d, J = 8.3 Hz, 12 H), 8.67 (d, J = 8.3 Hz, 12 H), 8.62 (d, J = 5.9 Hz, 24 H), 8.52 (d, J = 8.7 Hz, 12 H), 8.20 (t, J = 8.4 Hz, 12 H), 7.84 (d, J = 5.68 Hz, 24 H), 7.80–7.75 (m, 36H), 7.49 (m, 24 H). ^{13}C NMR (126 MHz, CD_3CN, RT):

160.0, 159.9, 155.5, 154.0, 151.6, 146.6, 143.8, 140.1, 139.7, 138.7, 138.4, 130.5, 128.9, 128.5, 126.4, 125.9, 125.1. ESI-MS: *m/z* 994.23 ($[Fe_4\mathbf{11}_6 + 14PF_6]^{6+}$), $C_{252}H_{180}F_{84}Fe_4N_{36}P_{14}$, calculated 994.13; 831.35 ($[Fe_4\mathbf{11}_6 + 13PF_6]^{7+}$), $C_{252}H_{180}F_{78}Fe_4N_{36}P_{13}$, calculated 831.40; 709.30 ($[Fe_4\mathbf{11}_6 + 12PF_6]^{8+}$), $C_{252}H_{180}F_{72}Fe_4N_{36}P_{12}$, calculated 709.35; 614.38 ($[Fe_4\mathbf{11}_6 + 11PF_6]^{9+}$) $C_{252}H_{180}F_{66}Fe_4N_{36}P_{11}$, calculated 614.43.

Cage 12 (Triflimide salt)

Triflimide salt **12** (16.0 mg, 13.6 µmol) was dissolved in CH_3CN (3.4 mL) and then iron (II) triflimide (5.7 mg, 9.3 µmol) was added causing the solution to turn ruby red. The homogenous solution was sonicated for 30 minutes and then stirred at 70°C for 24 h. The reaction mixture was cooled to room temperature and then Et_2O (6.0 mL) was added which resulted in a red solid. The heterogenous mixture was centrifuged followed by removal of the supernatant. The solid was resuspended in Et_2O (6.0 mL) with the help of sonication followed by centrifugation and decantation of the supernatant to obtain the red solid. The process was repeated two more times followed by air drying to obtain **12** as a red solid. ^{1}H NMR (400 MHz, CD_3CN, RT): 9.11 (d, *J* = 6.7 Hz, 24 H), 8.73 (d, *J* = 8.3 Hz, 12 H), 8.66 (d, *J* = 8.3 Hz, 12 H), 8.59 (d, *J* = 6.7 Hz, 24 H), 8.50 (d, *J* = 8.4 Hz, 12 H), 8.20 (t, *J* = 7.4 Hz, 12 H), 7.85–7.70 (m, 60 H), 7.49 (m, 24 H). ^{13}C NMR (126 MHz, CD_3CN, RT): 160.0, 159.7, 155.4, 151.5, 146.5, 143.7, 140.0, 139.6, 138.6, 138.2, 130.3, 128.9, 128.4, 126.3, 125.1, 121.9, 119.8.

Cage 12 (Sulphate salt)

A solution of K_2SO_4 (6.8 mg, 39 µmol) in D_2O (500 µL) was treated with **12**•2Cl (2.6 mg, 3.8 µmol) and $FeSO_4$•$7H_2O$ (13 mM, 200 µL, 2.5 µmol) dissolved in D_2O. The reaction mixture was sonicated for 1 hour and then stirred at 50°C for 24 hours during which the solution changed colour from cloudy yellow to clear ruby red. Acetone (5.0 mL) was added to the reaction mixture which results in a red precipitate. The heterogeneous mixture was centrifuged, the supernatant decanted, and the pellet was air dried to give **12** as red solid. ^{1}H NMR (600 MHz, D_2O, RT): 9.39 (d, *J* = 5.8 Hz, 24 H), 8.88 (d, *J* = 7.6 Hz, 12 H), 8.82 (br. s, 24 H), 8.77 (d, *J* = 7.6 Hz, 12 H), 8.61 (d, *J* = 7.9 Hz, 12 H), 8.25 (br., 12 H), 7.90–7.85 (m, 36H), 7.75 (d, *J* = 6.8 Hz, 12 H), 7.70 (d, *J* = 7.44 Hz, 12 H), 7.53 (br., 12 H). ^{13}C NMR (126 MHz, D_2O, Acetone as a standard, RT): 158.8, 158.2, 154.0, 151.2, 150.3, 145.0, 142.4, 138.7, 137.9, 137.5, 137.3, 128.7, 127.2, 126.9, 124.9, 124.1, 123.7.

Cage 13 (Hexafluorophosphate salt)

A mixture of CB[7] (28.7 mg, 24.7 µmol) and **11**•2Cl (17.0 mg, 24.7 µmol) was dissolved in D_2O (6.0 mL) using a heat gun and sonication and the 1:1 stoichiometric ratio was confirmed by measuring the ^{1}H NMR integrals for each component. The solution was heated to 80°C and treated with NH_4PF_6 (44.8 mg, 275 µmol) which caused the formation of an yellow precipitate. The heterogenous mixture was stirred at 80°C for 30 minutes before cooling to room temperature, centrifuged, and the supernatant decanted. The moist solid was resuspended in water (2.0 mL) with the help of sonication followed by centrifugation and decantation. The process was repeated two more times and then the solid (44.1 mg, 86%) was dried on high vacuum overnight. A sample of **11**•CB[7] hexafluorophosphate salt (2.3 mg, 1.1 µmol) was dissolved in CH_3CN (0.15 mL) and then a solution of $FeOTf_2$ (50 µL, 16 mM in CH_3CN) was added which caused the solution to turn ruby red. The reaction mixture was sonicated for 30 min. and then stirred at 60° C for 24 h. The reaction mixture was cooled to room temperature and then Et_2O (7.0 mL) was added which resulted in a red precipitate. The red precipitate was obtained by centrifugation followed by decanting of the supernatant. The moist solid was resuspended in Et_2O (2.0 mL) with the help of sonication followed by centrifugation and decantation of the supernatant. The process was repeated two more times and then air dried to give **13** as a red solid. Compound **13** was redissolved in CH_3CN (0.5 mL) and excess NH_4PF_6 (1.8 mg, 11 µmol) was added. Et_2O (6.0 mL) was added to the solution causing **13** to precipitate. After centrifugation and decantation of the supernatant, **13**•$20PF_6$ was collected as red solid. The red solid was resuspended in Et_2O (2.0 mL) with the help of vortexing and collected by centrifugation and decantation. This process was repeated two additional time to ensure the removal of excess NH_4PF_6. The red solid was then air dried to yield **13**•$20PF_6$. IR (ATR, cm^{-1}): 3493 m, 3115 w, 2920 w, 2361 w, 1733s, 1634 m, 1465s, 1422 m, 1375 m, 1375 m, 1320 m, 1281 m, 1227s, 1188s, 1029 m, 967 m, 823 m, 801s, 757 m, 671 m. ^{1}H NMR (600 MHz, CD_3CN, RT): 9.20–9.00 (m, 24 H), 8.80–8.45 (m, 57 H), 8.20 (br., 20 H), 8.00–7.75 (m, 53 H), 7.47 (br., 28 H), 7.02 (br. s, 7 H), 5.56 (br., 26 H), 5.35–5.15 (m, 26 H), 4.01 (br., 26 H). ^{13}C NMR (126 MHz, CD_3CN, RT): 165.6, 160.2, 159.8, 156.2, 155.2, 151.4, 148.8, 146.6, 139.9, 139.2, 128.9, 128.4, 126.3, 123.9, 71.6, 53.4. ESI-MS: 1163.73 ($[Fe_4\mathbf{11}_6 + 2CB[7] + 13PF_6]^{7+}$), $C_{336}H_{264}F_{78}Fe_4N_{92}O_{28}P_{13}$, calculated 1163.64; 1145.43 ($[Fe_4\mathbf{11}_6 + 3CB[7] + 12PF_6]^{8+}$), $C_{378}H_{306}F_{72}Fe_4N_{120}O_{42}P_{12}$, calculated 1145.48; 1002.16 ($[Fe_4\mathbf{11}_6 + 3CB[7] + 11PF_6]^{9+}$), $C_{378}H_{306}F_{66}Fe_4N_{120}O_{42}$

P_{11}, calculated 1002.10; 1000.27 ([Fe_4**11**$_6$ + 2CB[7] + 12PF_6]$^{8+}$), $C_{336}H_{264}F_{72}Fe_4N_{92}O_{28}P_{12}$, calculated 1000.07; 887.3467 ([Fe_4**11**$_6$ + 3CB[7] + 10PF_6]$^{10+}$), $C_{378}H_{306}F_{60}Fe_4N_{120}O_{42}P_{10}$, calculated 887.39; 872.89 ([Fe_4**11**$_6$ + 2CB[7] + 11PF_6]$^{9+}$), $C_{336}H_{264}F_{66}Fe_4N_{92}O_{28}P_{11}$, calculated 872.84; 854.72 ([Fe_4**11**$_6$ + 1CB[7] + 12PF_6]$^{8+}$), $C_{294}H_{222}F_{72}Fe_4N_{64}O_{14}P_{12}$, calculated 854.77; 793.49 ([Fe_4**11**$_6$ + 3CB[7] + 9PF_6]$^{11+}$), $C_{378}H_{306}F_{54}Fe_4N_{120}O_{42}P_9$, calculated 793.54; 771.11 ([Fe_4**11**$_6$ + 2CB[7] + 10PF_6]$^{10+}$), $C_{336}H_{264}F_{60}Fe_4N_{92}O_{28}P_{10}$, calculated 771.06; 743.64 ([Fe_4**11**$_6$ + 1CB[7] + 11PF_6]$^{9+}$), $C_{294}H_{222}F_{66}Fe_4N_{64}O_{14}P_{11}$, calculated 743.69.

Cage 13 (Triflimide salt)

A mixture of CB[7] (10.4 mg, 8.9 µmol) and **11**•2Cl (6.2 mg, 9.0 µmol) was dissolved in D_2O (7.0 mL) and the 1:1 stoichiometric ratio was confirmed by measuring the ^{1}H NMR integrals for each component. The solution was heated to 80°C and treated with $LiNTf_2$ (0.5 mL, 0.2 mM in CH_3CN) which caused the formation of an orange-brown precipitate. The heterogenous mixture was stirred at 80°C for 30 minutes. The heterogenous mixture was cooled to room temperature, centrifuged, and the supernatant decanted. The moist solid was resuspended in water (1.0 mL) with the help of sonication followed by centrifugation and decantation. The process was repeated two more times and then the solid (16.5 mg, 81%) was dried on high vacuum overnight. A sample of **11**•CB[7] triflimide salt (7.9 mg, 4.3 µmol) was dissolved in CH_3CN (0.5 mL) and then a solution of $Fe(NTf_2)_2$ (0.5 mL, 6.2 mM in CH_3CN) was added which caused the solution to turn ruby red. The reaction mixture was sonicated for 30 min. and then stirred at 70°C for 24 h. The reaction mixture was cooled to room temperature and then Et_2O (10.0 mL) was added which resulted in a red precipitate. The red precipitate was obtained by centrifugation followed by decanting of the supernatant. The moist solid was resuspended in Et_2O (5.0 mL) with the help of sonication followed by centrifugation and decantation of the supernatant. The process was repeated two more times and then air dried to give **13** as a red solid. ^{1}H NMR (600 MHz, CD_3CN, RT): 9.25–9.00 (br. m), 8.85–8.45 (m), 8.19 (br.s), 8.0–7.70 (br. m), 7.49 (br. m), 6.99 (br. s), 5.55 (br.), 5.17 (br.), 3.94 (br.). ^{13}C NMR (200 MHz, CD_3CN, RT): 160.0, 156.2, 155.3, 153.7, 151.5, 149.0, 143.7, 140.0, 139.5, 138.6, 130.3, 128.9, 128.4, 126.3, 125.1, 123.7, 123.3, 121.7, 120.1, 71.5, 53.3.

Compound 15

A solution of H_2O (16.7 mL), MeOH (5.1 mL), and THF (5.1 mL) was purged with N_2 for 15 min. and then compound **14** (0.154 g, 0.66 mmol), **9** (0.158 g, 0.72 mmol), and potassium carbonate (2.62 g, 29.2 mmol) were added to solution. The reaction mixture was heated and stirred at 70°C under N_2 for 24 hours. The reaction mixture was then cooled to room temperature and solvents were removed under vacuum. The crude solid was dissolved in CH_2Cl_2 (100 mL) and partitioned against aq. KOH (1 mM, 100 mL) in a separatory funnel. The organic layer was collected and dried over Na_2SO_4 prior to removing the solvent by rotary evaporation. Compound **15** was purified by column chromatography (SiO_2, DCM/EtOAc/NEt_3 50:50:3). ^{1}H NMR analysis revealed residual triphenyl phosphine so the solid was triturated three times with hexanes (10 mL) to give **15** (0.103 g, 64%) as a brown solid. The ^{1}H NMR of **15** recorded in $CDCl_3$ matches with data reported previously [108].

Compound 16 (Chloride salt)

A suspension of **15** (95.0 mg, 0.38 mmol) and **1** (102 mg, 0.18 mmol) in EtOH (25 mL) was heated at reflux for 3 days during which the solution turned brown. The reaction mixture was concentrated by rotary evaporation (to ≈10 mL) and then poured into THF (200 mL) and then stirred for 2 hours which gave an orange-brown precipitate. The precipitate was obtained by filtration and then washed on the frit with THF (100 mL) to give **16** (96.0 mg, 77%) as an orange-brown solid. M.p. > 300° C. IR (ATR, cm^{-1}): 3368 m, 3007 w, 1629 m, 1601 m, 1601 m, 1583 m, 1546 w, 1531 w, 1512 w, 1492 w, 1459 m, 1436 m, 1386 m, 1342 w, 1257 w, 991 w, 825s, 810s. ^{1}H NMR (400 MHz, DMSO-d_6, RT) 9.80 (d, J = 5.6 Hz, 4 H), 9.07 (d, J = 5.6 Hz, 4 H), 8.89 (d, J = 6.1 Hz, 2H), 8.81 (s, 2H), 8.77 (d, J = 6.1 Hz, 2H), 8.49 (d, J = 6.1 Hz, 2H), 8.35 (d, J = 8.6 Hz, 2H), 8.19 (d, J = 8.6 Hz, 4 H), 8.03 (dt, J = 6.1 and 1.8 Hz, 4 H), 7.97 (dd, J = 6.1 and 1.8 Hz, 2H), 7.54 (dt, J = 6.1 and 1.8 Hz, 2H). ^{13}C NMR (126 MHz, DMSO-d_6): 156.0, 154.7, 150.3, 149.2, 149.0, 146.5, 146.1, 142.8, 140.4, 137.7, 128.8, 126.4, 125.8, 124.7, 122.0, 120.9, 118.1. ESI-MS (ESI, sample dissolved in H_2O): *m/z* 309.1 ([M]$^{2+}$), $C_{42}H_{30}N_6$, calculated 309.4.

Compound 16 (Hexafluorophosphate salt)

Compound **16** (chloride) was transformed into the hexafluorophosphate salt by dissolving **16** · 2Cl (15.4 mg, 22.3 µmol) in water (5.0 mL) and heating to 80°C followed by the addition of NH_4PF_6 (39.7 mg, 244 µmol) was resulted in the formation of a precipitate. Heterogenous mixture was stirred at 80°C for 30 minutes. The heterogenous mixture was cooled to room temperature, centrifuged, and the supernatant was decanted to give a moist solid. The moist solid was suspended in

water (2.0 mL) with the help of sonication, followed by centrifugation, and removal of the supernatant. This process was repeated three times to remove excess NH_4PF_6 and then the solid **16**•2PF_6 (13.8 mg, 68%) was dried under high vacuum. M.p. > 300°C. IR (ATR, cm^{-1}): 3133 w, 3070 w, 2925 w, 2361 w, 2339 w, 1733 w, 1638 m, 1602w, 1585 m, 1568 w, 1541 w, 1515 w, 1491 w, 1460 m, 1440 m, 1387 m, 1352 w, 1216 w, 1188 w, 1132 w, 1096 w, 1039 w, 1007 w, 827s, 796s, 752 w, 739 w, 716 w, 707 w, 662 w. ^{1}H NMR (600 MHz, CD_3CN, RT): 9.29 (d, *J* = 6.5, 4 H), 8.84 (m, 4 H), 8.75–8.65 (m, 6 H), 8.52 (d, *J* = 7.9 Hz, 2H), 8.23 (d, *J* = 8.4, 4 H), 7.96 (m, 6 H), 7.80 (d, *J* = 3.5 Hz, 2H), 7.46 (t, *J* = 5.0 Hz, 2H). ^{13}C NMR (126 MHz, CD_3CN): 157.9, 156.4, 151.3, 150.4, 147.8, 146.8, 143.1, 138.4, 130.4, 128.4, 126.4, 125.5, 123.0, 122.0, 119.6. ESI-MS (ESI, sample dissolved in CH_3CN): *m/z* 309.1 ($[M]^{2+}$), $C_{42}H_{30}N_6$, calculated 309.4.

Compound 16 (Triflimide salt)

Counter anion exchange from chloride to triflimide was performed by dissolving **16** · 2Cl (16.3 mg, 23.6 µmol) in water (5 mL) and heated to 80°C, followed by addition of excess $LiNTf_2$ (70.4 mg, 245 µmol) which resulted in the formation of an brown precipitate. The heterogenous mixture was centrifuged, the supernatant was decanted, and the moist solid was resuspended in water (4.0 mL) with the help of sonication followed by centrifugation and the decantation of the precipitate. The process was repeated 2 more times to give **16**•2NTf_2 after drying under high vacuum (19.2 mg, 69%). M.p. > 300°C. IR (ATR, cm^{-1}): 3119 w, 3064 w, 1634 m, 1601 m, 1584 m, 1547 w, 1495 w, 1472 w, 1459 w, 1432 w, 1390 w, 1347s, 1226 m, 1174s, 1130s, 1051s, 1006w, 993 w, 826 m, 790 m, 762 w,790 m, 762 w, 739 m, 706 w. ^{1}H NMR (600 MHz, CD_3CN, RT): 9.28 (d, *J* = 6.8, 4 H), 8.84 (m, 4 H), 8.75–8.65 (m, 6 H), 8.52 (d, *J* = 8.0 Hz, 2H), 8.23 (d, *J* = 8.6, 4 H), 7.97 (m, 6 H), 7.80 (dd, *J* = 1.6, 5.0 Hz, 2H), 7.46 (t, *J* = 5.0 Hz, 2H). ^{13}C NMR (126 MHz, CD_3CN): 151.4, 151.2, 150.2, 147.9, 146.7, 143.7, 143.0, 138.7, 130.4, 128.5, 126.4, 125.5, 123.1, 122.1, 122.0, 119.9, 119.7. ESI-MS (ESI, sample dissolved in CH_3CN): *m/z* 309.1 ($[M]^{2+}$), $C_{42}H_{30}N_6$, calculated 309.4.

Cubic cage 17 (Hexafluorophosphate salt)

The obtained hexafluorophosphate salt of **17** (5.7 mg, 26.3 µmol) was dissolved in CH_3CN (1.0 mL) followed by the addition of iron (II) triflate (10.7 mM, 0.5 mL, 5.4 µmol) in CH_3CN which resulted in a colour change to dark purple. The reaction mixture was sonicated for 30 minutes followed by stirring at 60°C for 24 h. The reaction mixture is cooled to room temperature and then Et_2O (6.0 mL) is added which results in a purple precipitate. The heterogenous mixture is centrifuged, the supernatant decanted, and the moist solid is resuspended in Et_2O (6.0 mL) with the help of sonication followed by centrifugation and decantation. The process is repeated two more times. Compound **17** was redissolved in CH_3CN (0.5 mL) and excess NH_4PF_6 (12.9 mg, 79.1 µmol) was added. Et_2O (6.0 mL) was added to the solution causing **17** to precipitate. After centrifugation and decantation of the supernatant, **17**•40PF_6 was collected as purple solid. The purple solid was resuspended in Et_2O (2.0 mL) with the help of vortexing and collected by centrifugation and decantation. This process was repeated two additional time to ensure the removal of excess NH_4PF_6. The purple solid was then air dried to yield **17**•40PF_6 (7.2 mg, 78%). IR (ATR, cm^{-1}): 3124 w, 2087w, 1633 w, 1615 w, 1476 w, 1440 w, 1400 w, 1218 w, 1029 w, 817s, 739 m. ^{1}H NMR (600 MHz, CD_3CN, RT): 9.30 (br. s, 48 H), 8.96 (br. s, 24 H), 8.84 (br. s, 24 H), 8.74 (br. s, 48 H), 8.30–8.24 (m, 72 H), 8.06 (br. s, 48 H), 7.81 (br. s, 24 H), 7.62–7.53 (m, 72 H). ^{13}C NMR (126 MHz, CD_3CN, RT): 165.7, 161.1, 157.5, 155.6, 151.8, 149.4, 146.8, 144.6, 140.2, 130.8, 128.6, 126.7.

Cubic cage 17 (Triflimide salt)

The obtained triflimide salt of **17** (15.3 mg, 13.0 µmol) was dissolved in CH_3CN (3.3 mL) followed by the addition of iron (II) triflimide (5.3 mg, 8.6 µmol) which resulted in a colour change to dark purple. The reaction mixture was sonicated for 30 minutes followed by stirring at 70°C for 24 h. The reaction mixture is cooled to room temperature and then Et_2O (7.0 mL) is added which results in a red precipitate. The heterogenous mixture is centrifuged, the supernatant decanted, and the moist solid is resuspended in Et_2O (6.0 mL) with the help of sonication followed by centrifugation and decantation. The process is repeated two more times and then solid **17** is air dried. ^{1}H NMR (400 MHz, CD_3CN, RT): 9.29 (br. s, 48 H), 8.94 (br. m, 24 H), 8.83 (br. m, 24 H), 8.72 (br., 48 H), 8.35–8.20 (m, 72 H), 8.04 (br., 48 H), 7.79 (br. s, 24 H), 7.70–7.45 (m, 72 H). ^{13}C NMR (126 MHz, CD_3CN, RT): 160.9, 159.9, 158.9, 155.4, 151.5, 149.7, 146.7, 144.4, 140.3, 139.9, 130.7, 128.4, 126.6, 123.3, 121.8, 119.7, 177.6.

Cubic cage with CB[7] (18 · 40PF_6)

A mixture of CB[7] (22.7 mg, 19.5 µmol) and **16**•2Cl (13.4 mg, 19.4 µmol) was dissolved in D_2O (5.0 mL) by sonication and using a heat gun. The 1:1 stoichiometric ratio was confirmed by the integrals for each component in the ^{1}H NMR spectrum. The solution was heated

to 80°C and treated with NH_4PF_6 (32.4 mg, 199 μmol) which caused the formation of a tan precipitate. The heterogenous mixture continued to stir at 80°C for 30 minutes. The heterogenous mixture was centrifuged, the supernatant decanted, and the moist solid was resuspended in water (2.0 mL) followed by centrifugation and decantation two additional times. The solid was then dried at high vacuum overnight to yield the triflimide salt (34.0 mg, 85%). Complex **16·CB[7]** hexafluorophosphate salt (3.3 mg, 0.16 μmol) was dissolved in CH_3CN (1.0 mL). The solution was treated with $Fe(OTf)_2$ (22 mM, 50 μL, 0.11 μmol) dissolved in acetonitrile which gave a dark purple solution when added. The reaction mixture was sonicated for 30 min. and then stirred at 70°C for 24 h. The reaction mixture is cooled to room temperature and then Et_2O (6.0 mL) is added which results in a purple precipitate. The heterogenous mixture is centrifuged, the supernatant decanted, and the moist solid is then resuspended in Et_2O followed by centrifugation and decantation of the precipitate. Compound **18** was redissolved in CH_3CN (0.5 mL) and excess NH_4PF_6 (1.0 mg, 6.1 μmol) was added. Et_2O (6.0 mL) was added to the solution causing **18** to precipitate. After centrifugation and decantation of the supernatant, **18**·40PF_6 was collected as purple solid. The purple solid was resuspended in Et_2O (2.0 mL) with the help of vortexing and collected by centrifugation and decantation. This process was repeated two additional time to ensure the removal of excess NH_4PF_6. The purple solid was then air dried to yield **18**·40PF_6. IR (ATR, cm^{-1}): 3486 m, 3123 w, 2916 m, 2849 w, 2362 w, 2338 w,1735s, 1631 m, 1463s, 1423 m, 1375 m, 1319 m,1280 m, 1227s, 1188s, 1029 m, 967 m, 841 m, 822 m, 800s, 757 m, 671 w. ^{1}H NMR (600 MHz, CD_3CN, RT): 9.30 (d, J = 5.6 Hz), 9.00–8.65 (m), 8.50–8.00 (m), 8.00–7.40 (m), 5.75–5.55 (br. m), 5.35–5.15 (br. m), 4.10–3.90 (br. m). ^{13}C NMR (126 MHz, CD_3CN, RT): 161.3, 159.8, 156.2, 148.8, 146.6, 144.5, 140.6, 139.7, 130.6, 128.4, 126.5, 124.0, 121.8, 119.7, 71.5, 53.2.

Cubic cage with CB[7] (18 · 40NTf_2^-)

A mixture of CB[7] (13.8 mg, 11.9 μmol) and **16**·2Cl (9.6 mg, 13.9 μmol) was dissolved in D_2O (4.0 mL) and the 1:1 stoichiometric ratio was confirmed by the integrals for each component in the ^{1}H NMR spectrum. Solid $LiNTf_2$ (43.6 mg, 152 μmol) was added to the solution which resulted in the formation of a precipitate. The heterogenous mixture was centrifuged, the supernatant decanted, and the moist solid was resuspended in water (2.0 mL) followed by centrifugation and decantation. The solid was then dried at high vacuum overnight to yield the triflimide salt (25.0 mg, 97%). Complex **16·CB[7]** triflimide salt (7.3 mg, 3.9 μmol) and $Fe(NTf_2)_2$ (1.8 mg, 2.9 μmol) were dissolved in CH_3CN (1.0 mL) which gave a dark purple solution. The reaction mixture was sonicated for 30 min. and then stirred at 70°C for 24 h. The reaction mixture is cooled to room temperature and then Et_2O (6.0 mL) is added which results in a purple precipitate. The heterogenous mixture is centrifuged, the supernatant decanted, and the moist solid is then resuspended in Et_2O followed by centrifugation and decantation of the precipitate. The process is repeated two more times followed by air drying to give **18** · 40$(NTf_2)^-$ as a purple solid. ^{1}H NMR (400 MHz, CD_3CN, RT): 9.29 (br. s), 9.00–8.60 (m), 8.45–7.95 (m), 7.95–7.40 (m), 5.75–5.55 (br. m), 5.35–5.15 (br. m), 4.10–3.90 (br. m). ^{13}C NMR (126 MHz, CD_3CN, RT): 161.3, 159.8, 156.2, 148.8, 146.6, 144.5, 140.6, 139.7, 130.6, 128.4, 126.5, 124.0, 121.8, 119.7, 71.5, 53.2.

Acknowledgments

We thank the National Institutes of Health (CA226830) and the National Science Foundation (CHE1807486) for financial support. K.B. thanks the University of Maryland for a Department of Education GAANN fellowship (P200A150033).

Disclosure of potential conflicts of interest

The authors have no competing interests to declare.

Funding

This work was supported by the National Cancer Institute (NCI) [CA226830]; National Science Foundation [CHE1807486]; U.S. Department of Education [P200A1150033].

ORCID

Xiaopeng Li http://orcid.org/0000-0001-9655-9551
Lyle Isaacs http://orcid.org/0000-0002-4079-332X

References

[1] Barrow SJ, Kasera S, Rowland MJ, et al. Cucurbituril-based molecular recognition. Chem Rev. **2015**;115:12320–12406.
[2] Rekharsky MV, Inoue Y. Complexation thermodynamics of cyclodextrins. Chem Rev. **1998**;98:1875–1917.
[3] Diederich F. Complexation of neutral molecules by cyclophane hosts. Angew Chem Int Ed. **1988**;27:362–386.
[4] Dale EJ, Vermeulen NA, Juricek M, et al. Supramolecular explorations: exhibiting the extent of extended cationic cyclophanes. Acc Chem Res. **2016**;49:262–273.

[5] Gutsche CD. Calixarenes. Acc Chem Res. **1983**;16:161–170.
[6] Cram DJ. The design of molecular hosts, guests, and their complexes. Angew Chem Int Ed. **1988**;27:1009–1020.
[7] Ogoshi T, Yamagishi T-A, Nakamoto Y. Pillar-shaped macrocyclic hosts pillar[n]arenes: new key players for supramolecular chemistry. Chem Rev. **2016**;116:7937–8002.
[8] Xue M, Yang Y, Chi X, et al. Pillararenes, a new class of macrocycles for supramolecular chemistry. Acc Chem Res. **2012**;45:1294–1308.
[9] Wu J-R, Yang Y-W. New opportunities in synthetic macrocyclic arenes. Chem Commun. **2019**;55:1533–1543.
[10] Stella VJ, Rao VM, Zannou EA, et al. Mechanisms of drug release from cyclodextrin complexes. Adv Drug Deliv Rev. **1999**;36:3–16.
[11] Ghale G, Nau WM. Dynamically analyte-responsive macrocyclic host–fluorophore systems. Acc Chem Res. **2014**;47:2150–2159.
[12] Yu Y, Rebek J. Reactions of folded molecules in water. Acc Chem Res. **2018**;51:3031–3040.
[13] Anslyn EV. Supramolecular analytical chemistry. J Org Chem. **2007**;72:687–699.
[14] Meadows MK, Anslyn EV. Three tales of supramolecular analytical chemistry. Macrocyclic Supramol Chem. **2016**:92–126.
[15] Walker S, Oun R, McInnes FJ, et al. The potential of cucurbit[n]urils in drug delivery. Isr J Chem. **2011**;51:616–624.
[16] Ma X, Zhao Y. Biomedical applications of supramolecular systems based on host-guest interactions. Chem Rev. **2015**;115:7794–7839.
[17] Zhang H, Liu Z, Zhao Y. Pillararene-based self-assembled amphiphiles. Chem Soc Rev. **2018**;47:5491–5528.
[18] Ogoshi T, Harada A. Chemical sensors based on cyclodextrin derivatives. Sensors. **2008**;8:4961–4982.
[19] Border SE, Pavlovic RZ, Zhiquan L, et al. Removal of nerve agent simulants from water using light-responsive molecular baskets. J Am Chem Soc. **2017**;139:18496–18499.
[20] Wang W, Finnegan TJ, Lei Z, et al. Tuning the allosteric sequestration of anticancer drugs for developing cooperative nano-antidotes. Chem Commun. **2020**;56:1271–1274.
[21] Zhou J, Yu G, Huang F. Supramolecular chemotherapy based on host-guest molecular recognition: a novel strategy in the battle against cancer with a bright future. Chem Soc Rev. **2017**;46:7021–7053.
[22] Zhang X, Cheng Q, Li L, et al. Supramolecular therapeutics to treat the side effects induced by a depolarizing neuromuscular blocking agent. Theranostics. **2019**;9:3107–3121.
[23] Huang Q, Zhao H, Shui M, et al. Heparin reversal by an oligoethylene glycol functionalized guanidinocalixarene. Chem Sci. **2020**;11:9623–9629.
[24] Chang Y, Chen J-Y, Yang J, et al. Targeting the cell membrane by charge-reversal amphiphilic pillar[5]arene for the selective killing of cancer cells. ACS Appl Mater Interfaces. **2019**;11:38497–38502.
[25] Kassem S, Van Leeuwen T, Lubbe AS, et al. Artificial molecular motors. Chem Soc Rev. **2017**;46:2592–2621.
[26] Adam JM, Bennett DJ, Bom A, et al. Cyclodextrin-derived host molecules as reversal agents for the neuromuscular blocker rocuronium bromide: synthesis and structure-activity relationships. J Med Chem. **2002**;45:1806–1816.
[27] Bom A, Bradley M, Cameron K, et al. A novel concept of reversing neuromuscular block: chemical encapsulation of rocuronium bromide by a cyclodextrin-based synthetic host. Angew Chem Int Ed. **2002**;41:265–270.
[28] Trinh T, Cappel JP, Geis PA, et al. (Procter and Gamble Company, USA), Uncomplexed cyclodextrin solutions for odor control on inanimate surfaces, especially fabrics. WO9605358A1. 1996.
[29] Stella VJ, Rajewski RA. Cyclodextrins: their future in drug formulation and delivery. Pharm Res. **1997**;14:556–567.
[30] Lagona J, Mukhopadhyay P, Chakrabarti S, et al. The cucurbit[n]uril family. Angew Chem Int Ed. **2005**;44:4844–4870.
[31] Nau WM, Florea M, Assaf KI. Deep inside cucurbiturils: physical properties and volumes of their inner cavity determine the hydrophobic driving force for host–guest complexation. Isr J Chem. **2011**;51:559–577.
[32] Masson E, Ling X, Joseph R, et al. Cucurbituril chemistry: a tale of supramolecular success. RSC Adv. **2012**;2:1213–1247.
[33] Shetty D, Khedkar JK, Park KM, et al. Can we beat the biotin–avidin pair?: cucurbit[7]uril-based ultrahigh affinity host–guest complexes and their applications. Chem Soc Rev. **2015**;44:8747–8761.
[34] Lee JW, Samal S, Selvapalam N, et al. Cucurbituril homologues and derivatives: new opportunities in supramolecular chemistry. Acc Chem Res. **2003**;36:621–630.
[35] Bush ME, Bouley ND, Urbach AR. Charge-mediated recognition of n-terminal tryptophan in aqueous solution by a synthetic host. J Am Chem Soc. **2005**;127:14511–14517.
[36] Smith LC, Leach DG, Blaylock BE, et al. Sequence-specific, nanomolar peptide binding via cucurbit[8]uril-induced folding and inclusion of neighboring side chains. J Am Chem Soc. **2015**;137:3663–3669.
[37] Bosmans RPG, Briels JM, Milroy L-G, et al. Supramolecular control over split-luciferase complementation. Angew Chem Int Ed. **2016**;55:8899–8903.
[38] Dsouza RN, Pischel U, Nau WM. Fluorescent dyes and their supramolecular host/guest complexes with macrocycles in aqueous solution. Chem Rev. **2011**;111:7941–7980.
[39] Liu S, Ruspic C, Mukhopadhyay P, et al. The cucurbit[n]uril family: prime components for self-sorting systems. J Am Chem Soc. **2005**;127:15959–15967.
[40] Macartney DH. Encapsulation of drug molecules by cucurbiturils: effects on their chemical properties in aqueous solution. Isr J Chem. **2011**;51:600–615.
[41] Gamal-Eldin MA, Macartney DH. Cucurbit[7]uril host-guest complexations of steroidal neuromuscular blocking agents in aqueous solution. Can J Chem. **2014**;92:243–249.
[42] Ganapati S, Grabitz SD, Murkli S, et al. Molecular containers bind drugs of abuse in vitro and reverse the

hyperlocomotive effect of methamphetamine in rats. ChemBioChem. **2017**;18:1583–1588.
[43] Kaifer AE. Toward reversible control of cucurbit[n]uril complexes. Acc Chem Res. **2014**;47:2160–2167.
[44] Ko YH, Kim E, Hwang I, et al. Supramolecular assemblies built with host-stabilized charge-transfer interactions. Chem Commun. **2007**;1305–1315. DOI:10.1039/B615103E
[45] Zhang X, Xu X, Li S, et al. A systematic evaluation of the biocompatibility of cucurbit[7]uril in mice. Sci Rep. **2018**;8:1–7.
[46] Cao L, Sekutor M, Zavalij PY, et al. Cucurbit[7]uril.Guest pair with an attomolar dissociation constant. Angew Chem Int Ed. **2014**;53:988–993.
[47] Isaacs L. Stimuli responsive systems constructed using cucurbit[n]uril-type molecular containers. Acc Chem Res. **2014**;47:2052–2062.
[48] Del Barrio J, Horton P, Lairez D, et al. Photocontrol over cucurbit[8]uril complexes: stoichiometry and supramolecular polymers. J Am Chem Soc. **2013**;135:11760–11763.
[49] Gao C, Kwong CHT, Sun C, et al. Selective decoating-induced activation of supramolecularly coated toxic nanoparticles for multiple applications. ACS Appl Mater Interfaces. **2020**;12:25604–25615.
[50] Ma D, Zhang B, Hoffmann U, et al. Acyclic cucurbit[n]uril-type molecular containers bind neuromuscular blocking agents in vitro and reverse neuromuscular block in vivo. Angew Chem Int Ed. **2012**;51:11358–11362.
[51] Yang H, Yuan B, Zhang X, et al. Supramolecular chemistry at interfaces: host-guest interactions for fabricating multifunctional biointerfaces. Acc Chem Res. **2014**;47:2106–2115.
[52] Liu J, Lan Y, Yu Z, et al. Cucurbit[n]uril-based microcapsules self-assembled within microfluidic droplets: a versatile approach for supramolecular architectures and materials. Acc Chem Res. **2017**;50:208–217.
[53] Aqdot Home Page; [cited 2020 May 6]. Available from: https://aqdot.com
[54] Rebek J. Molecular behavior in small spaces. Acc Chem Res. **2009**;42:1660–1668.
[55] Jordan JH, Gibb BC. Molecular containers assembled through the hydrophobic effect. Chem Soc Rev. **2015**;44:547–585.
[56] Yoshizawa M, Klosterman JK, Fujita M. Functional molecular flasks: new properties and reactions within discrete, self-assembled hosts. Angew Chem Int Ed. **2009**;48:3418–3438.
[57] Chakrabarty R, Mukherjee PS, Stang PJ. Supramolecular coordination: self-assembly of finite two- and three-dimensional ensembles. Chem Rev. **2011**;111:6810–6918.
[58] Brown CJ, Toste FD, Bergman RG, et al. Supramolecular catalysis in metal–ligand cluster hosts. Chem Rev. **2015**;115:3012–3035.
[59] Furukawa H, Cordova KE, O'Keeffe M, et al. The chemistry and applications of metal-organic frameworks. Science. **2013**;341:1230444.
[60] Zarra S, Wood DM, Roberts DA, et al. Molecular containers in complex chemical systems. Chem Soc Rev. **2015**;44:419–432.
[61] Della Rocca J, Liu D, Lin W. Nanoscale metal–organic frameworks for biomedical imaging and drug delivery. Acc Chem Res. **2011**;44:957–968.
[62] Sumida K, Rogow DL, Mason JA, et al. Carbon dioxide capture in metal–organic frameworks. Chem Rev. **2012**;112:724–781.
[63] Wilson BH, Loeb SJ. Integrating the mechanical bond into metal-organic frameworks. Chem. **2020**;6:1604–1612.
[64] Roy I, Limketkai B, Botros YY, et al. Cyclodextrin metal-organic frameworks: from the research laboratory to the marketplace. Acc Chem Res. **2020**;53:2762.
[65] Li Q, Zhang W, Miljanic OS, et al. Docking in metal-organic frameworks. Science. **2009**;325:855–859.
[66] Li Q, Sue C-H, Basu S, et al. A catenated strut in a catenated metal-organic framework. Angew Chem Int Ed. **2010**;49:6751–6755, S6751/6751-S6751/6719.
[67] Tian J, Zhou T-Y, Zhang S-C, et al. Three-dimensional periodic supramolecular organic framework ion sponge in water and microcrystals. Nat Commun. **2014**;5:5574.
[68] Tian J, Xu Z-Y, Zhang D-W, et al. Supramolecular metal-organic frameworks that display high homogeneous and heterogeneous photocatalytic activity for h2 production. Nat Commun. **2016**;7:11580.
[69] Zhang Y-C, Xu Z-Y, Wang Z-K, et al. A woven supramolecular metal-organic framework comprising a ruthenium bis(terpyridine) complex and cucurbit[8]uril: enhanced catalytic activity toward alcohol oxidation. ChemPlusChem. **2020**;85:1498–1503.
[70] Das G, Sharma SK, Prakasam T, et al. A polyrotaxanated covalent organic network based on viologen and cucurbit[7]uril. Commun Chem. **2019**;2:1–9.
[71] Mal P, Breiner B, Rissanen K, et al. White phosphorus is air-stable within a self-assembled tetrahedral capsule. Science. **2009**;324:1697.
[72] Benyettou F, Prakasam T, Ramdas Nair A, et al. Potent and selective in vitro and in vivo antiproliferative effects of metal–organic trefoil knots. Chem Sci. **2019**;10:5884–5892.
[73] Zheng Y-R, Suntharalingam K, Johnstone TC, et al. Encapsulation of Pt(iv) prodrugs within a Pt(ii) cage for drug delivery. Chem Sci. **2015**;6:1189–1193.
[74] Qiao Y, Zhang L, Li J, et al. Switching on supramolecular catalysis via cavity mediation and electrostatic regulation. Angew Chem Int Ed. **2016**;55:12778–12782.
[75] Samanta SK, Moncelet D, Briken V, et al. Metal-organic polyhedron capped with cucurbit[8]uril delivers doxorubicin to cancer cells. J Am Chem Soc. **2016**;138:14488–14496.
[76] Samanta SK, Quigley J, Vinciguerra B, et al. Cucurbit[7]uril enables multi-stimuli-responsive release from the self-assembled hydrophobic phase of a metal organic polyhedron. J Am Chem Soc. **2017**;139:9066–9074.
[77] Samanta SK, Moncelet D, Vinciguerra B, et al. Metal organic polyhedra: a click-and-clack approach toward targeted delivery. Helv Chim Acta. **2018**;101:e1800057.
[78] Nitschke JR. Construction, substitution, and sorting of metallo-organic structures via subcomponent self-assembly. Acc Chem Res. **2007**;40:103–112.

[79] Castilla AM, Ramsay WJ, Nitschke JR. Stereochemistry in subcomponent self-assembly. Acc Chem Res. **2014**;47:2063–2073.
[80] Rodríguez J, Mosquera J, Couceiro JR, et al. Anion recognition as a supramolecular switch of cell internalization. J Am Chem Soc. **2017**;139:55–58.
[81] Riddell IA, Smulders MMJ, Clegg JK, et al. Encapsulation, storage and controlled release of sulfur hexafluoride from a metal–organic capsule. Chem Commun. **2011**;47:457–459.
[82] Bolliger JL, Belenguer AM, Nitschke JR. Enantiopure water-soluble [fe4l6] cages: host–guest chemistry and catalytic activity. Angew Chem Int Ed. **2013**;52:7958–7962.
[83] Neelakandan PP, Jiménez A, Nitschke JR. Fluorophore incorporation allows nanomolar guest sensing and white-light emission in m4l6 cage complexes. Chem Sci. **2014**;5:908–915.
[84] Foster JA, Parker RM, Belenguer AM, et al. Differentially addressable cavities within metal–organic cage-cross-linked polymeric hydrogels. J Am Chem Soc. **2015**;137:9722–9729.
[85] Biedermann F, Scherman OA. Cucurbit[8]uril mediated donor–acceptor ternary complexes: a model system for studying charge-transfer interactions. J Phys Chem B. **2012**;116:2842–2849.
[86] Ong W, Gómez-Kaifer M, Kaifer AE. Cucurbit[7]uril: a very effective host for viologens and their cation radicals. Org Lett. **2002**;4:1791–1794.
[87] Ong W, Kaifer AE. Salt effects on the apparent stability of the cucurbit [7] uril– methyl viologen inclusion complex. J Org Chem. **2004**;69:1383–1385.
[88] Wang W, Kaifer AE. Transfer of cationic cucurbit[7]uril inclusion complexes from water to non-aqueous solvents. Supramol Chem. **2010**;22:710–716.
[89] Kamogawa H, Sato S. Redox photochromism of arylviologen crystals. Bull Chem Soc Japan. **1991**;64:321–323.
[90] Fischer-Durand N, Rejeb SB, Le Goffic F. Synthesis of 4-benzidinyl butyric acid: a key intermediate for antibodies production against benzidin. Synth Commun. **1998**;28:963–970.
[91] Cheng W-C, Kurth MJ. The zincke reaction. A review. Org Prep Proced Int. **2002**;34:585,587–608.
[92] Percástegui EG, Mosquera J, Nitschke JR. Anion exchange renders hydrophobic capsules and cargoes water-soluble. Angew Chem Int Ed. **2017**;56:9136–9140.
[93] Schultz D, Nitschke JR. Choices of iron and copper: cooperative selection during self-assembly. Angew Chem Int Ed. **2006**;45:2453–2456.
[94] Meng W, Clegg JK, Thoburn JD, et al. Controlling the transmission of stereochemical information through space in terphenyl-edged Fe4L6 cages. J Am Chem Soc. **2011**;133:13652–13660.
[95] Ronson TK, Meng W, Nitschke JR. Design principles for the optimization of guest binding in aromatic-paneled feii4l6 cages. J Am Chem Soc. **2017**;139:9698–9707.
[96] Avram L, Cohen Y. Diffusion nmr of molecular cages and capsules. Chem Soc Rev. **2015**;44:586–602.
[97] Einstein A. Über die von der molekularkinetischen theorie der wärme geforderte bewegung von in ruhenden flüssigkeiten suspendierten teilchen. Ann Phys. **1905**;322:549–560.
[98] Mock WL, Shih NY. Structure and selectivity in host-guest complexes of cucurbituril. J Org Chem. **1986**;51:4440–4446.
[99] Liu Y, Yu Y, Gao J, et al. Water-soluble supramolecular polymerization driven by multiple host-stabilized charge-transfer interactions. Angew Chem Int Ed. **2010**;49:6576–6579.
[100] Kim J, Jung I-S, Kim S-Y, et al. New cucurbituril homologues: syntheses, isolation, characterization, and x-ray crystal structures of cucurbit[n]uril (n = 5, 7, and 8). J Am Chem Soc. **2000**;122:540–541.
[101] Amabilino DB, Stoddart JF. Interlocked and intertwined structures and superstructures. Chem Rev. **1995**;95:2725–2828.
[102] Mahata K, Frischmann PD, Würthner F. Giant electroactive m4l6 tetrahedral host self-assembled with fe(ii) vertices and perylene bisimide dye edges. J Am Chem Soc. **2013**;135:15656–15661.
[103] Glasson CRK, Meehan GV, Clegg JK, et al. A new feii quaterpyridyl m4l6 tetrahedron exhibiting selective anion binding. Chem Commun. **2008**;1190–1192. DOI:10.1039/b717740b
[104] Zhang Y, Crawley MR, Hauke CE, et al. Phosphorescent decanuclear bimetallic pt6m4 (m = zn, fe) tetrahedral cages. Inorg Chem. **2017**;56:4258–4262.
[105] Hauser A, Vef A, Adler P. Intersystem crossing dynamics in fe(ii) coordination compounds. J Chem Phys. **1991**;95:8710–8717.
[106] Clegg JK, Cremers J, Hogben AJ, et al. A stimuli responsive system of self-assembled anion-binding fe4l68+ cages. Chem Sci. **2013**;4:68–76.
[107] Browne C, Brenet S, Clegg JK, et al. Solvent-dependent host–guest chemistry of an fe8l12 cubic capsule. Angew Chem Int Ed. **2013**;52:1944–1948.
[108] Elmes RBP, Erby M, Bright SA, et al. Photophysical and biological investigation of novel luminescent ru(ii)-polypyridyl-1,8-naphthalimide tröger's bases as cellular imaging agents. Chem Commun. **2012**;48:2588–2590.